Atmos. Chem. Phys. Discuss., doi:10.5194/acp-2016-287, 2016
Manuscript under review for journal Atmos. Chem. Phys.
Published: 22 April 2016

Atmospheric Chemistry and Physics Discussions

Pivotal role of the North African Dipole Intensity (NAFDI) on alternate Saharan dust export over the North Atlantic and the Mediterranean, and relationship with the Saharan Heat Low and mid-latitude Rossby waves

E. Cuevas[1], A. J. Gómez-Peláez[1], S. Rodríguez[1], E. Terradellas[2], S. Basart[3], R. D. García[1,4], O. E. García[1], and S. Alonso-Pérez[5]

[1]{Izaña Atmospheric Research Centre (AEMET), Santa Cruz de Tenerife, Spain}

[2] {SDS-WAS Regional Centre (AEMET), Barcelona, Spain}

[3] {Earth Sciences Department, Barcelona Supercomputing Centre, Barcelona, Spain}

[4] {Air Liquide S.A., Delegación de Canarias, Candelaria, Santa Cruz de Tenerife, Spain}

[5] {Universidad Europea de Canarias, La Orotava, Santa Cruz de Tenerife, Spain}

Abstract

In this study, we revise the index that quantifies the North African Dipole Intensity (NAFDI), and explain its relationship with the Saharan Heat Low (SHL) and mid-latitude Rossby waves. We find outstanding similarities of meteorological patterns associated with the positive NAFDI and the SHL West-phase on the one hand, and with the negative NAFDI and the SHL East-Phase, on the other hand. We introduce the daily NAFDI index and the daily SHL West-East Displacement Index (SHLWEDI). The Pearson correlation coefficient between the daily SHLWEDI 1-day lagged and the daily NAFDI for the period 1980-2013 20 June – 17 September is fairly high (r = 0.77). The correlation reduces to 0.69 if the SHLWEDI is not lagged. We observe that the SHL West-phase is significantly more frequent than the SHL East-phase, and that the SHL is more intense during its East-phase. We find positive aerosol optical depth (AOD) anomalies in the Western Sahara during positive NAFDI / SHL West-phase, and negative AOD anomalies in the central and eastern Sahara during negative NAFDI / SHL East-phase. A significant positive (negative) NE-SW axis AOD

Atmos. Chem. Phys. Discuss., doi:10.5194/acp-2016-287, 2016
Manuscript under review for journal Atmos. Chem. Phys.
Published: 22 April 2016

Atmospheric Chemistry and Physics
Discussions

anomaly over the Subtropical North Atlantic for positive (negative) NAFDI is found. Remarkable patterns of positive (negative) AOD anomalies over the tropical Atlantic and the Central-Western Mediterranean during negative (positive) NAFDI are observed. The impact of mid-latitude Rossby waves on NAFDI variations depends on both the amplitude and phase of the Rossby wave at 200-300 hPa, which is quantified in this study by the daily Zonal Wind Anomaly at 300 hPa over South Morocco (ZWA300), and the penetration of the Rossby wave into the lower troposphere, quantified by the daily Omega at 500 hPa over Northwest Algeria (O500). The correlation of both ZWA300 and O500 with NAFDI is significant: 0.48 and 0.53, respectively, when we apply 5-day running means to the time series before calculating the correlation coefficients, and increases to 0.66 when a multi-linear regression is performed. The results suggest that ZWA300 drives almost one day in advance the NAFDI, whereas O500 might be ahead respect to NAFDI less than 12 hours. The power spectra of the NAFDI, SHL, ZWA300 and O500 times series in the intermediate time scale range (between 10 and 30 days) show 10 especially intense NAFDI spectral peaks, most of them also present in the SHLWEDI spectrum, finding that for many of the NAFDI/SHLWEDI peaks there is associated an O500 and/or ZWA300 peak. Our results indicate that the modes of oscillation of both the NAFDI and the SHL are driven by those mid-latitudes Rossby waves that go deep enough into the lower troposphere imposing their perturbation to the background meteorological fields. A comprehensive top-down conceptual model is introduced to explain the relationships between the NAFDI, the SHL and the mid-latitude Rossby waves and their impact in dust mobilization and transport in Northern Africa.

1 Introduction

Northern Africa, and specifically the Sahara desert, is the largest and most active dust source in the world (Ginoux et al., 2004, 2012; Huneeus et al., 2011). There are numerous studies dealing with mineral dust transport from the Sahara to the North Atlantic within the Saharan Air Layer (SAL) (e.g., Prospero and Carlson, 1997; Engelstaedter and Washington, 2007; Haywood et al., 2008, Ben-Ami et al., 2009; Adams et al., 2012; Prospero et al., 2014; Ridley et al., 2014) and its impacts on remote regions, i.e. the Caribbean, and the Americas (Perry et al., 1997; Prospero, 1999; Prospero and Lamb, 2003; Chiapello et al., 2005). The impact of Saharan dust over the Mediterranean has also been subject of numerous papers in recent years (e.g., Moulin et al., 1998; Kubilay et al., 2003; Pérez et al., 2006; Gerasopoulos et al., 2006;

Basart et al., 2009; Jilbert et al., 2010; Salvador et al., 2014; Marconi et al., 2014) addressing its impact on air quality (Rodríguez et al., 2001; Escudero et al., 2007a; 2007b; Querol et al., 2009), and ocean fertilization (Guerzoni et al., 1999; Gallisai et al., 2012; Ravelo-Pérez et al., 2016). However, dust transport over the North Atlantic and Mediterranean has been approached independently in most of the studies, disregarding the fact that the large pressure centres that modulate dust transport to both regions are basically the same. Both the Saharan heat low (SHL), widely analyzed in recent years (e.g. Lavaysse et al., 2009; 2010a; 2010b; 2011; 2013; 2015; Chauvin et al.; 2010), and the North African anticyclone (Rodríguez et al., 2015) are pressure centres whose variations in intensity, position and extension are key factors for activating dust emissions and transport to the North Atlantic and Mediterranean.

In the last years a great effort has been made to explain the most important dust mobilization mesoscale baroclinic processes driven, somehow, by the SHL. Among them, we could highlight the following mechanisms: dry boundary layer convection (Engelstaedter and Washington, 2007; Lavaysse et al., 2010a, and references therein), density currents (Marsham et al., 2008, and references therein; Schepanski et al., 2009; Chaboureau et al., 2016), low-level jets (LLJ) (Knippertz, 2008; Schepanski et al., 2009; Fiedler et al., 2013), strong winds and high turbulence associated to the Intertropical Convergence Zone (ITCZ) (Flamant et al., 2007; Bou Karam et al., 2008; Canut et al., 2010), and African easterly waves (AEWs) (Jones et al., 2003; Knippertz and Todd, 2010). However, although there is general agreement on the fact that changes in intensity and position of SHL play an important role in the atmospheric regional dust recirculation through the activation of the mesoscale baroclinic processes listed above, little is known about the physical processes that determine the variability in the position and intensity of the SHL. It is generally accepted that dust mobilization is mainly controlled by soil characteristics, surface conditions and surface wind speed. Dry soil conditions can be assumed as constant in central hyper-arid Sahara. Therefore, the main factor that modulates the activation of the multiple dust sources present in this region is the low-level wind variability.

Chauvin et al. (2010) found a relation between mid-latitude Rossby waves and the longitudinal position of the SHL. However, they did not explain the underlying physical mechanisms behind this relation. Applying Fourier Analysis to the linearized barotropic vorticity equation for a constant-density atmosphere, with a constant zonal flow, it is straightforward to obtain the dispersion relation for the free barotropic Rossby waves (e.g., Holton, 1992). However, the propagation of Rossby waves in the real atmosphere is a much

Atmos. Chem. Phys. Discuss., doi:10.5194/acp-2016-287, 2016
Manuscript under review for journal Atmos. Chem. Phys.
Published: 22 April 2016

Atmospheric Chemistry and Physics
Discussions

more complex issue. According to Pedlosky (1987), in the vertically stratified real atmosphere, a Rossby wave may be considered as barotropic if it has the same structure throughout the vertical column, except that the amplitude is affected by an exponential factor depending on height. These considerations apply for a static atmosphere or with a constant zonal velocity (Pedlosky, 1987). The use of more realistic models that consider a zonal background flow depending on latitude and height makes the calculation of Rossby waves much more complex since it requires solving numerically an eigenvalue problem of ordinary or partial differential equations with specific boundary conditions. The forced barotropic vorticity equation has been often used in the literature to study the longitudinal propagation of Rossby waves in the upper troposphere (e.g., Charney and Eliassen, 1949; Hoskins and Ambrizzi, 1993; Ambrizzi et al., 1995). Sometimes the Wentzel–Kramers–Brillouin (WKB) method has been used to try to understand, at least qualitatively, the behaviour observed in complex models and in reanalysis (e.g., Hoskins and Karoly, 1981; Karoly and Hoskins, 1982; Karoly, 1983; Hoskins and Ambrizzi, 1993; Petoukhov et al., 2013). Hsu and Lin (1992), Hoskins and Ambrizzi (1993), and Ambrizzi et al. (1995) showed that in the Northern Hemisphere there are waveguides for the propagation of Rossby waves in the upper troposphere. The propagation of Rossby waves through the North Atlantic and North African waveguide and the longitudinal position of the SHL are related each other according to Chauvin et al. (2010).

In this study, we start from the results obtained by Rodríguez et al. (2015) regarding the so-called North African Dipole Intensity (NAFDI). The NAFDI is the difference of geopotential height anomalies averaged over the subtropics and the tropics close to the Atlantic coast. Rodríguez et al. (2015) analyzed the relationship between the NAFDI and dust export to the Atlantic in August by using 28-year measurement data of in-situ dust concentrations at Izaña Observatory and satellite - TOMS and OMI Aerosol Index based - dust retrievals.

The major objectives of the present study are: 1) review the definition of the NAFDI index and assess the results obtained by Rodríguez et al. (2015) using complementary spatial fields of Aerosol Optical Depth (AOD) from MODIS retrievals and MACC (Monitoring Atmospheric Composition and Climate) reanalysis, and extending the analysis to every month of the summertime (June-August); 2) explore the role played by the NAFDI in dust transport to the Mediterranean basin, and its impact on dust source activation over the Sahara; 3) determine and analyse the physical mechanisms that link the NAFDI and the SHL on a daily

Atmos. Chem. Phys. Discuss., doi:10.5194/acp-2016-287, 2016
Manuscript under review for journal Atmos. Chem. Phys.
Published: 22 April 2016

basis, and 4) analyse the variations of Rossby waves (amplitude and phase) in the North-East Atlantic, identifying on a daily basis the physical mechanisms by which these waves modulate the NAFDI variations and hence, the SHL phases.

In Section 2, the observational and reanalysis datasets used in the study are described. The main results and discussion are tackled in Section 3: review of the NAFDI definition, dust transport and meteorological patterns associated with the NAFDI phases, and physical relationship between the NAFDI, the SHL and mid-latitude Rossby waves. Finally, in Section 4, the conclusions and the schematic conceptual model from hemispheric to meso-scale atmospheric mechanisms driving dust transport over Northern Africa are presented.

2 Data and methodology

2.1 MACC reanalysis

The 10-year MACC reanalysis for 2003–2012 (Innes et al., 2013) has been used in this study. The MACC reanalysis data can be downloaded from the European Centre for Medium-Range Weather Forecasts (ECMWF) at http://apps.ecmwf.int/datasets/data/macc-reanalysis/levtype=sfc/. In this study, we have used daily averages of AOD at 550 nm computed from the MACC data at 06, 09, 12, 15 and 18 UTC in the period 2003-01-01 to 2012-12-31.

A detailed description of the initial implementation of the aerosol modules for this reanalysis is given in Morcrette et al. (2009) for the modelling part, and in Benedetti et al. (2009) for the assimilation part. The physical parameterizations for the aerosol processes are modelled using the LOA/LMD-Z model (Boucher et al., 2002; Reddy et al., 2005). However, some modifications to the original schemes were introduced over the years (Morcrette et al., 2011). Five types of tropospheric aerosols are considered in the model: sea-salt, mineral dust, organic and black carbon, and sulphate aerosols. The MACC reanalysis was run at T255L60, which is an approximate 78 km × 78 km horizontal resolution with 60 vertical levels. Dust is treated as a chemically non-reactive component, which is externally mixed like all other aerosols in the MACC model. The data assimilation system used to produce the MACC reanalysis is based on a 2010 release of the ECMWF Integrated Forecasting System (IFS) (Cy36r1). The system includes a 4-dimensional variational analysis (4D-Var) with a 12-hour analysis window for O_3, CO, NO_2, SO_2, HCHO, and aerosols.

The output of the MACC reanalysis has been validated by the MACC-II VAL sub-project and the latest information has been reported by Eskes et al., 2014. The MACC reanalysis has already been used in several aerosol studies including mineral dust (e.g. Bellouin et al., 2013; Inness et al., 2013; Cesnulyte et al., 2014; Cuevas et al., 2015; Eskes et al., 2015).

2.2 Satellite (MODIS and MISR) data

The MODerate resolution Imaging Spectrometer (MODIS) onboard the NASA EOS (Earth Observing System) Terra and Aqua satellites (Salomonson et al., 1989) provides aerosol properties over both land (Kaufman et al., 1997) and ocean (Tanré et al., 1997) with a near-daily global coverage.

In this study we have used AOD-500 nm monthly averages for the period 2003-01-01 to 2012-12-31 from the MODIS Collection 6 atmosphere aerosol products available in the NASA LADS ftp server (ftp://ladsweb.nascom.nasa.gov/allData/6/). MODIS Collection 6 includes a merged product, which uses Deep Blue (DB) retrievals to fill in gaps in the Dark Target/ocean (DT) dataset, with extended coverage to vegetated surfaces, as well as bright land, and improved surface reflectance models, aerosol optical models, and cloud screening, and simplified quality assurance flags (Hsu et al., 2013; Sayer et at., 2013). The new features of Collection 6 are especially important for our study since much of the geographic domain we use in our analysis covers North Africa, a region in which we have to identify both dust transport and dust sources over surfaces of high reflectivity on which the AOD retrieval is difficult.

Multi-angle Imaging Spectro Radiometer (MISR) instrument, flying aboard the NASA Earth Observing System's Terra satellite (http://www-misr.jpl.nasa.gov/), gets a global coverage every 9 days with revisit time between 2 and 9 days depending on latitude. MISR can retrieve aerosol properties over bright desert areas due to its unique capability of multi-wavelength observations at forward and backward directions (Kahn el al., 2010). According to Kahn et al. (2010), between 70 and 75% of the MISR AOD retrievals differ less than 0.05, or 20% from the corresponding AERONET ones.

In section 3.3 we have used monthly-averaged values of the MODIS daily merged AOD product (MYD08_M3_V6), and MISR monthly AOD at 555nm (MIL3MAE_V4), for the period 2003-2012, produced with the Giovanni online data system, developed and maintained by the NASA GES DISC (http://giovanni.gsfc.nasa.gov/).

2.3 ERA-Interim Reanalysis

ERA-Interim is the latest global atmospheric reanalysis produced by the ECMWF, extending from 1979 to present. ERA-Interim is based on a 2006 release of the IFS (Cy31r2). As the MACC reanalysis, it is run at a T255L60 resolution. The system includes a 4-dimensional variational analysis (4D-Var) with a 12-hour analysis window. A detailed description of ERA-Interim Reanalysis is given in Dee et al. (2011).

In this study we have used daily-averaged fields of temperature, wind, and geopotential height at standard levels from 1000 to 500 hPa in the period 2003-01-01 to 2012-12-31.

2.4 NCEP/NCAR Reanalysis

The NCEP/NCAR Reanalysis Project is a joint project between the National Centers for Environmental Prediction (NCEP) and the National Center for Atmospheric Research (NCAR). A description of the NCEP/NCAR reanalysis can be found in (Kalnay et al., 1996).

In this study we have used NCEP/NCAR daily and monthly-averaged data with a spatial resolution of 2.5° latitude x 2.5° longitude, in the period 1980-2013. No fundamental differences have been found in our analysis when using NCEP/NCAR reanalysis or ERA-Interim Reanalysis. So, we have used the latter, which has a better spatial resolution, in plots and results focused on Northern Africa linked to AOD outputs from MACC and MODIS retrievals. However, for larger geographical scales and for computing correlations and regressions between NAFDI and other atmospheric parameters we have used the user-friendly NCEP/NCAR reanalysis web page interface (http://www.esrl.noaa.gov/psd/products/) for reasons of easiness and efficiency in calculations.

2.5 Hysplit trajectories

Two sets of daily 48-hour-long air back-trajectories beginning at 12:00 UTC, with a 1-hour time resolution, were computed using the Hybrid Single Particle Lagrangian Integrated Trajectory Model (HYSPLIT) version 4.0 (Stein et al., 2015). The arrival points were set at 30ºN 15ºW 700 hPa (subtropical North Atlantic) and 37ºN, 4ºE 700 hPa (Western Mediterranean), for each of the two sets, respectively.

Daily backward trajectories were calculated for the summer months (June, July and August) in the period 2003-2012. Wind fields from the NCEP/NCAR reanalysis meteorological data set (Kalnay et al. 1996) were used. The vertical model velocity was used.

The percentage of backward trajectories that passed over North Africa was calculated for each month, and for each summer, in the 2003-2012 period, distinguishing between NAFDI positive and negative phases. In order to calculate this percentage, we calculated the fraction of time that each backward trajectory resides in the geographic sector bounded by the parallels 20°N and 36°N, and the meridians 18°W and 50°E, using a similar approach to that used by Alonso-Pérez et al. (2007) for calculating the Saharan Index. When that fraction of time is 25% or greater, the associated backward trajectory is flagged as influenced by African air masses, and its starting day is considered as potentially affected by the African CBL.

3 Results and discussion

3.1 A review and some remarks on the NAFDI definition

The definition of NAFDI introduced by Rodríguez et al. (2015) was made with the aim to analyze dust transport from the Sahara to the North Atlantic Ocean. Thus, the points chosen to calculate the geopotential height derivative anomaly at 700 hPa were selected over Morocco and Mali, almost along the same meridian (around 7ºW). Since the scope of the present study covers a much larger region, we have proceeded to revise the definition of the index that quantifies NAFDI.

We have computed the correlation map between the geopotential height at 700 hPa over the selected point over Morocco and the geopotential height field at the same level (Figure 1a). This figure shows that the geopotential heights over the two regions (over Morocco and Mali) used to define the NAFDI correlate positively, and therefore, their variations are not completely independent. Moreover, the associated regression plot (Figure 1b) shows a pattern of isolines similar to that of the correlation plot. This isoline pattern indicates that the geostrophic wind anomaly has not only a westward component, but also a significant northerly component. For these reasons we have decided to improve slightly the definition of the NAFDI index by selecting the meridional point at the same latitude of that chosen by Rodríguez et al. (2015) but shifted eastwards symmetrically to the Greenwich meridian, specifically at 5°-7.5ºE (North Nigeria) instead of 6°-8ºW. Notice that with the new

Atmos. Chem. Phys. Discuss., doi:10.5194/acp-2016-287, 2016
Manuscript under review for journal Atmos. Chem. Phys.
Published: 22 April 2016

definition, the correlation between the 700 hPa geopotential at the selected points is zero (Figure 1a), that is, the geopotential variations are independent. As shown in the correlation maps between the geopotential height at 700 hPa and both the NAFDI index defined by Rodríguez et al (2015) (Figure 1c) and the improved NAFDI index for the latter (Figure 1d), there is a higher correlation on the northernmost point and more negative correlations in the tropical belt. Moreover, the geopotential height derivative anomaly that the improved NAFDI index provides is calculated along a line that is perpendicular to the geostrophic wind anomaly and crosses the core of the SHL, where dust is lifted-up. Further information supporting these facts is provided in Sections 3.2 and 3.3. The corresponding regression plot between the improved NAFDI and the geopotential height at 700 hPa for August months is shown in Supplement S1.

The total dust concentrations ($dust_T$) measured at the Izaña Atmospheric Observatory in August months and the NAFDI time series from 1987 to 2014 present indeed a Pearson correlation coefficient (r) of 0.67 when using the original NAFDI index definition (Rodríguez et al., 2015), whereas r = 0.72 when using the improved NAFDI index. These results indicate that the outstanding results from Rodríguez et al. (2015) might be even better by using this improved index. The improved NAFDI index will be referred to as the NAFDI From now on, replacing that established by Rodríguez et al. (2015). The monthly NAFDI values for the period 1948-2015 are available at http://izana.aemet.es/dataseries/. In this study the NAFDI is used for grouping and averaging spatial distributions of AOD from both MODIS retrievals and MACC reanalysis and some atmospheric parameters related with atmospheric mineral dust exportation from North Africa to the Mediterranean and the subtropical Atlantic. Specifically, we use monthly average values of the NAFDI for June, July and August in different time periods within the longest used period 1980-2013. These summer months are classified, in turn, into three groups: positive NAFDI (> +0.4), negative NAFDI (< -0.4) and neutral NAFDI (values between -0.4 and +0.4). This classification is used to group different values of atmospheric parameters described below. The NAFDI values corresponding to June, July and August for each year of the period 2003-2012 are shown in Supplement S2.

We have also calculated a daily NAFDI for 20 June - 17 September that will be used in Sections 3.3 and 3.4 to discuss the relationship between the NAFDI, the SHL and mid-latitude Rossby waves. The Daily-NAFDI has been calculated as follows:

$$NAFDI_i = \frac{1}{10}\left(\left(\Phi^i_{Mo} - <\Phi>_{Mo}\right) - \left(\Phi^i_{Ni} - <\Phi>_{Ni}\right)\right) \quad \text{Equation 1}$$

Atmos. Chem. Phys. Discuss., doi:10.5194/acp-2016-287, 2016
Manuscript under review for journal Atmos. Chem. Phys.
Published: 22 April 2016

where,

- Φ^i_{Mo} is the NCEP Reanalysis daily mean geopotential height at 700hPa in central Morocco region (30°N, 5°W) for day 'i'.
- Φ^i_{Ni} is the NCEP Reanalysis daily mean geopotential height at 700hPa in North Nigeria region (12.5°N, 5°E) for day 'i'
- $<\Phi>$ indicates average of the geopotential for the considered day (i) of the year during the reference period 1981-2010, and subsequent application of a 29-day running mean to the average, in order to remove the small residual random component.

3.2 Dust transport and meteorological patterns associated with the NAFDI phases

The MODIS AOD anomalies for summer months (June, July and August) with positive and negative NAFDI phases in the period 2003-2012 are shown in Figure 2.

Large patterns of AOD anomalies, associated to long-range transport of dust out of Northern Africa, are remarkable. First, we detect a significant positive AOD anomaly that follows a ENE-WSW axis on the subtropical Atlantic under positive NAFDI, which agrees with a positive anomaly of easterly winds between 925 and 700 hPa under positive NAFDI (see Supplement S3), and with results of Rodríguez et al. (2015) using NCEP reanalysis wind data for August in the period 1987-2014. Our results also confirm, and extend its validity to the whole summer period, the relationship between the NAFDI and averaged TOMS and OMI AI data averaged over the so called Subtropical North Atlantic (SNA) found by Rodríguez et al. (2015). This positive (negative) AOD anomaly on the subtropical Atlantic during positive (negative) NAFDI is very small in June, and increases considerably in July and August (Figure 2). A second remarkable pattern is the positive AOD anomaly observed over the tropical Atlantic during negative NAFDI (the opposite under the positive phase). In this case, the anomaly is stronger in June than in July and August. The third major contrast between the AOD patterns in the two phases of NAFDI is found on the Central-Western Mediterranean, where positive (negative) AOD anomalies occur during negative (positive) NAFDI. This pattern is especially clear in June, the summer month in which dust intrusions in the Central-Western Mediterranean are more frequent (Marconi et al., 2014).

We must highlight the fact that we find months with both positive and negative NAFDI values in the summer period of the same year, but the AOD-anomalies patterns found in months with the same phase of NAFDI are the same regardless of their time location within the summer season. This suggests that there are some well-defined dust-transport patterns on these regions, which are basically modulated by the NAFDI, and therefore by the North African high, beyond dust transport modulation over the subtropical North Atlantic reported by Rodríguez et al. (2015).

Additionally, there are AOD anomalies over Northern Africa. Figure 2 shows positive AOD anomalies in or near North African dust source regions, especially over Algeria and Libya, and to a lesser extent over Niger, Egypt, Sudan, and the Sahel region during negative NAFDI months, which become regions with negative AOD anomalies for positive NAFDI months. Note also that the first transport pattern mentioned previously extends inland with less intensity over all the subtropical West coast of Northern Africa. We suggest, therefore, that the NAFDI might also modulate, somehow, numerous mesoscale processes that, in turn, activate dust sources in these regions.

Complementarily, we have also calculated the AOD anomalies from MACC reanalysis for the two phases of the NAFDI, during the same period (2003-2012), for the same months of summer, and in the same way as the AOD anomalies from MODIS were calculated (Figure 3). The results, in general and ignoring small-scale details, are very similar to those obtained with MODIS. In both cases, the same structures for the most intense AOD anomalies are observed for each phase of the NAFDI although in the MACC case they are remarkably smoothed. In Supplement S4, averaged AOD anomalies from MODIS and MACC for summers with positive and negative NAFDI phases in the period 2003-2012 are shown.

The summer period in the Sahel region coincides with the rainy season with frequent dust emitted by wet mesoscale convective events (Marticorena et al., 2010) associated to the monsoon, which are not well captured by MACC (Cuevas et al., 2014). This is especially clear during positive NAFDI, while during negative NAFDI, MACC captures dust in the Sahel region what requires further analysis which is out of the scope of this paper.

In spite of the significant limitations of the MACC reanalysis, due to its relatively low resolution and the fact that convective processes and other mesoscale atmospheric processes are not parameterized, it provides important information that helps us to interpret the structures found in the AOD anomalies.

Atmos. Chem. Phys. Discuss., doi:10.5194/acp-2016-287, 2016
Manuscript under review for journal Atmos. Chem. Phys.
Published: 22 April 2016

Atmospheric Chemistry and Physics
Open Access
Discussions

The relatively good agreement between MODIS and MACC reanalysis at large scale, both on sea and land, tell us that these AOD-anomaly structures are basically modulated by atmospheric drivers operating at synoptic scale because, otherwise, the MACC reanalysis would not have been able to reproduce them. It is noted that the ECMWF IFS uses external data of aerosol optical depth at 550 nm retrieved from MODIS (Level 2, collection 5) instruments on board of Terra and Aqua satellites, which are assimilated into the model. However, MODIS AOD assimilation has not been applied over highly reflective surfaces, such as deserts where there is no sufficient contrast to discern the aerosol signal. In our case, a good agreement between MODIS Deep blue AOD and MACC reanalysis AOD is also observed over desert areas where no MODIS AOD data is assimilated. Moreover, the agreement between MODIS and MACC reanalysis confirms the suitability of MACC for climatological studies, like the present one.

The fact that AOD positive anomalies over the subtropical North Atlantic correspond systematically with dust free conditions over the Mediterranean basin, and vice versa, indicates that the dust transport processes over both regions are modulated by the same pressure systems which activate mineral dust advection towards one or another region as if it were a three-port two-position valve.

The ECMWF reanalysis monthly mean wind fields at 700 hPa (Figure 4) , which is the level at which the most effective dust transport into the North Atlantic occurs (Rodríguez et al., 2015), show for positive NAFDI stronger NE/NNE winds over a band extending over central Algeria, northern Mauritania and Western Sahara that prolongs into the subtropical North Atlantic. This is consistent with the positive AOD anomaly observed by MODIS (Figure 2) and provided by MACC (Figure 3). On the other hand, for negative NAFDI we observe stronger Westerlies over the Mediterranean and increased air flow from Northern Africa towards western and central Mediterranean. In order to confirm and quantify this distinct air mass transport depending on the NAFDI phase, we have computed the HYSPLIT daily backward trajectories with arrival points 30ºN 15ºW 700 hPa (North Atlantic) and 37ºN, 4ºE 700 hPa (Western Mediterranean) for the period 2003-2012. For each day, we have flagged the air mass at a destination point as potentially affected by the African CBL, if the corresponding backward trajectory has travelled at least during 12 hours above the African continent (i.e., fraction of time ≥ 25%). The corresponding daily statistics of African air masses at the Subtropical North Atlantic and the Western Mediterranean are expressed in

Atmos. Chem. Phys. Discuss., doi:10.5194/acp-2016-287, 2016
Manuscript under review for journal Atmos. Chem. Phys.
Published: 22 April 2016

Table 1 as monthly-mean relative frequencies for June, July and August for the period 2003-2012, and for each NAFDI phase.

Table 1. Monthly averaged frequency of "African air masses" arriving to the subtropical North Atlantic and the Western Mediterranean for June, July and August and positive and negative NAFDI based on daily HYSPLIT backwards trajectories ending at 30ºN 15ºW 700 hPa (subtropical North Atlantic) and 37ºN, 4ºE 700 hPa (Western Mediterranean) for the period 2002-2013.

Month and NAFDI phase	**Frequency (%) Subtropical North Atlantic**	**Frequency (%) Western Mediterranean**
June NAFDI +	15.0	45.0
June NAFDI -	3.3	67.8
July NAFDI +	31.6	67.1
July NAFDI -	24.2	74.2
August NAFDI +	34.4	49.5
August NAFDI -	12.9	65.6

In the subtropical North Atlantic the frequency of African air masses is between 7.4% and 21.5% higher during positive NAFDI than under negative NAFDI, while in the Western Mediterranean it happens just the opposite, finding higher frequency of African air masses during negative NAFDI (between 7.1% and 22.8% higher).

These patterns of African air masses transport into the North Atlantic with positive NAFDI, and to the central / western Mediterranean with negative NAFDI are consistent over time as we can see from the correlation maps between NAFDI and 700 hPa zonal (for the Atlantic) and meridional (for the Mediterranean) wind components for the period 1980-2013 (see Supplement S5). Quite similar correlations are found in the longer period 1948-2013 (not shown here).

The ECMWF zonal wind longitude-height cross-section along the 28°N parallel (Figure 5), just over the Canary Islands, where Rodríguez et al. (2015) observed maximum dust concentration under positive NAFDI, shows that in June there exists a vertical column above the coast of Africa in which dominates the Westerly wind component (positive values), preventing the transport of potentially dust-laden air from the African CBL to the Atlantic in both phases of the NAFDI. However, in July and August the situation is quite different: while for negative NAFDI we find a similar zonal wind-pattern than for June, for positive NAFDI the zonal wind component, between 900 and 700 hPa, becomes Easterly (negative values), allowing the transport of Saharan air masses over the North Atlantic. In fact, the NAFDI acts as a valve controller that closes or opens the air passage in Westward direction. In July and August, the Central Western Sahara (CWS) is characterized by strong and frequent mineral dust storms and by a deep CBL that favours the vertical mixing and the accumulation of lifted dust till heights of around 6 km (Cuesta et al., 2009; Guirado et al, 2014). So, the positive NAFDI pattern favours dust-laden African air masses transport over the subtropical North Atlantic. This is due largely to the weakening of the eastern branch of the Azores anticyclone during positive NAFDI (compared with negative NAFDI), as discussed below, which virtually disappears between 10° and 20° W at 700 hPa (Figure 5).

In the central-western Mediterranean the meridional wind latitude-height cross-section along the 9°E meridian indicates the opposite situation. For positive NAFDI there is a clear preponderance of the Northerly wind component (above the 900 hPa level) inhibiting the entry of African air masses into the Mediterranean. However, for negative NAFDI there is a strong Southerly wind component in June, and to a lesser extent, the same situation occurs in July and August, indicating a higher probability of dust intrusions into the Mediterranean (Figure 6). The Southerly wind component is observed over the boundary layer (above 900 hPa level), in agreement with other studies (e.g. Marconi et al., 2014) and found at higher altitudes as we move northward (from 900 to 500 hPa) in good agreement with results of Mona et al. (2006) who found that dust layer extended from 2.5 to 5.9 km height over south Italy using lidar measurements. For this reason, in-situ PM_{10} (particulate matter with particles smaller than 10 microns in diameter) stations are not always sensitivity enough for mineral dust transport into the Mediterranean basin.

After obtaining these results, the question is: which are the 700 hPa pressure patterns associated with this dual behaviour corresponding to positive and negative NAFDI? We have found that in June it does not exist, indeed, significant differences between the 700 hPa geopotential patterns associated to the two phases of NAFDI (Figure 7). However, in July and

Atmos. Chem. Phys. Discuss., doi:10.5194/acp-2016-287, 2016
Manuscript under review for journal Atmos. Chem. Phys.
Published: 22 April 2016

August we observe a marked difference. In the negative NAFDI phase a strong NE-SW trough axis extending over the Atlantic to the west of Europe and North Africa is observed. This trough separates further the Azores anticyclone from the North African anticyclone, displacing the latter to positions further East over the continent, and causing the Azores anticyclone to elongate slightly to the NE. On the contrary, in the positive NAFDI phase, the centres of both anticyclones strengthens and are closer, giving the impression that both merge into a single large anticyclone extending along much of the Atlantic and North Africa. It is worthy to emphasize here that the so-called Saharan or North African high is a distinct high system independent of the Azores North Atlantic anticyclone.

The 700 hPa geopotential height pattern found during negative NAFDI, characterized by a strong anticyclone over Algeria and a deep trough west of Europe, is exactly the 700 hPa geopotential pattern established by Varga et al. (2014) to explain the Saharan dust intrusions in the Western and Central Mediterranean. This is also the same pattern found by Gkikas et al. (2015) in their Cluster 2, which accounts for 51% of all desert aerosol intrusions in the whole Mediterranean basin. We can therefore say that the NAFDI modulates the main meteorological pattern causing mineral dust from the Sahara to the Central and Western Mediterranean, found in previous studies.

The deep trough we see over the eastern North Atlantic with negative NAFDI is not an exclusive feature of this level. We have calculated correlation maps between NAFDI and the geopotential heights at different levels between 1000 and 200 hPa, which show for July and August quite similar correlation patterns at 850, 700, 500 and 200 hPa (Supplement S6), and even footprints of those patterns at 1000 hPa, suggesting that the NAFDI variations might be governed by mid-latitude barotropic Rossby waves. These results aimed us to dedicate a sub-section (3.4) to the causal relationship between Rossby waves and the NAFDI.

3.3 Relationship between NAFDI and the Saharan Heat Low (SHL) and its impact on meso-scale dust sources

SHL is the denomination given to the West African Heat Low (WAHL) when is located over the Western Sahara desert (between the Hoggar and the Atlas mountains) during summertime (from 20 June till 17 September). The SHL is characterized by high surface air temperature and low surface pressure (a thermal low) with a broad low-level cyclonic circulation and a

Atmos. Chem. Phys. Discuss., doi:10.5194/acp-2016-287, 2016
Manuscript under review for journal Atmos. Chem. Phys.
Published: 22 April 2016

Atmospheric Chemistry and Physics Discussions

mid-level anticyclonic circulation above (the mid-level thermal high associated to the low-level thermal low) centred around 5°W-25°N (Lavaysse et al., 2009; Wang et al., 2015).

In our analysis we find spatial patterns of some meteorological variables for each phase of the NAFDI, which closely resemble those found in previous studies of the SHL West and East phases. The most remarkable are: 1) the relative position and extension of the Azores anticyclone during NAFDI positive and negative phases (Figure 7) shows some similarities with the Chauvin et al. (2010) description: a large extension over Europe during the SHL West-phase, and a retreat to its subtropical Atlantic position during the SHL East-phase ; 2) the positive (negative) 1000 hPa temperature anomaly over Morocco and Western Sahara during positive (negative) NAFDI (Figure 8) is very similar to the warm (cold) anomaly over Morocco during the SHL West- (East-) phase reported by Chauvin et al. (2010); 3) the stronger Etesian and northerly low level winds over Libya found, mainly in July and August (850 hPa), during positive NAFDI and the larger entrance of northerly low-level winds into the interior of Western Sahara during negative NAFDI (Figure 9) correspond to the increased ventilation over Libya observed during SHL West-phase, and with an increased ventilation over Morocco and Western Sahara during SHL East-phase, respectively (Chauvin et al., 2010, Roehrig et al., 2011). These striking similarities in meteorological patterns between the positive NAFDI and SHL West-phase, on the one hand, and between the negative NAFDI and SHL East-Phase, on the other hand, suggest us that there should be a close relationship between the NAFDI and the SHL position. This relationship is analyzed, physically explained, and quantified below.

The WAHL location is defined by Lavaysse et al. (2009) in terms of the low-level atmospheric thickness (LLAT) between 925 and 700 hPa. They computed the LLAT for each point of the domain (20°W-30°E, 0°-40°N) and day (06:00 UTC) using re-analysis fields (ECMWF ERA-40). The LLAT is proportional to the mean temperature (where the integration is performed over the vertical variable *Log[p]*) of the air located between both pressure levels. The authors identified the location of the WAHL as that of the 10% upper values in the daily probability distribution of LLAT in the mentioned domain. As stated before, during the period 20 June - 17 September of each year, the WAHL is located over the Sahara and is called SHL. Using an EOF (Empirical Orthogonal Function) analysis performed only over areas detected and tracked as SHL during the season, Lavaysse et al. (2013) quantified the West-East displacement (called “pulsation” by these authors) of the SHL (see

Fig. 5c and 5d in Lavaysse et al. (2013)), being the frequencies of pulsation higher than 1/25 day^{-1}. However, as far as we know, the atmospheric processes that produce these pulsations have not yet been explained in detail.

To understand the causes of the SHL pulsations we have to bear in mind the fact that above the SHL (centred ~20°-22°N), is located the Saharan high, which is actually slightly displaced to the north with respect to the SHL with its centre at ~ 25ºN (Chen, 2005). The shifts and intensity of this mid-level anticyclone are driven, as we have seen, by NAFDI. Below we explain that the temporal evolution of the NAFDI and the West-East displacement of the SHL are physically connected, corresponding positive NAFDI to West SHL displacement, and negative NAFDI to East SHL displacement.

In order to prove this relationship, and using the NCEP reanalysis for the period 1980-2013, we define the daily SHL West-East Displacement Index (SHLWEDI) as:

$$SHLWEDI = \left[(T_W - < T_W >) - (T_E - < T_E >)\right] \qquad \text{Equation 2}$$

where T_W is the air temperature at 850 hPa, 25°N and 12.5°W, T_E is the air temperature at 850 hPa, 20°N and 7.5°E, and < > indicates averaging of the temperature of the considered day of the year for the reference period 1981-2010 and subsequent application of a 29-day running mean to the averages in order to remove the small residual random component. These geographical points have been selected using the locations of the maximum and minimum of the dipolar pattern that corresponds to the EOF of the SHL location obtained by Lavaysse et al. (2013) (see their Fig. 5c). The Pearson correlation coefficient between the daily SHLWEDI and the daily NAFDI for the period 1980-2013 20 June – 17 September is 0.69, which is quite high. In case only the daily western temperature anomaly is considered when computing the correlation with the daily NAFDI, it takes the value 0.67. This is due to the high anti-correlation between the western and eastern temperature anomalies (the correlation coefficient between the daily SHLWEDI and the western temperature anomaly is 0.91). We have also computed approximately the Pearson correlation coefficients between the daily SHLWEDI and the eigenvalue time series (ERA-I) plotted in Fig. 6c of Lavaysse et al. (2013) for the period 2007-2011 20 June – 17 September, obtaining a correlation of -0.74 (the negative sign is due to the fact that the Lavaysse's eigenvalue is positive for SHL East displacement whereas SHLWEDI is positive for SHL West displacement).

Atmos. Chem. Phys. Discuss., doi:10.5194/acp-2016-287, 2016
Manuscript under review for journal Atmos. Chem. Phys.
Published: 22 April 2016

Atmospheric Chemistry and Physics Discussions
Open Access

Figure 9 shows the mean wind speed and vector fields at 850 hPa for the three summer months with positive and negative NAFDI (similar results are observed for the 925 hPa fields; see Supplement S7). For negative NAFDI, the air arriving to the subtropical 10-20º W stripe comes from more northerly latitude in the North Atlantic and follows a more meridional direction than for positive NAFDI. This means the air arriving to this region under negative NAFDI is colder, what results in a negative advection of geopotential thickness. Since the absolute value of the thickness advection is maximum in the 10°-20º W stripe (due to the relative maximum in the meridional wind), a NE-SW through separating the Atlantic and North African highs at 700 hPa is generated, experiencing the latter a slightly eastward shift (see Figure 7). This meteorological pattern favours hot air from the SHL being transported to the Mediterranean at this 700 hPa level. When there is a transition from a negative to a positive NAFDI, the meridional negative advection of geopotential thickness strongly decreases in absolute value and the two highs at 700 hPa approach one another. The North African high transports hot air from above the SHL towards the west, acting in this western region like an upper barrier for thermal convection, which therefore heats a shallower depth of the lower troposphere, and thereby increases the temperature in this region. This makes the SHL and the coupled thermal high at 700 hPa to propagate westwards and to approach the Azores high. The intense ageostrophic wind component at 700 hPa (which is due to the fact that this pressure level is within a deep North African CBL) allows upper SAL air masses arrive till the region of influence of the Azores high, where these air masses are transported by the geostrophic wind into the North Atlantic region. The advection of hot Saharan air across the subtropical North Atlantic also contributes to increase the geopotentical thickness of the region located between the Azores and North Africa highs, merging them into an apparent single 700 hPa anticyclone extended across much of the North Atlantic and North Africa.

Figure 8 shows the anomaly of temperature at 1000 hPa in June, July and August for positive and negative NAFDI. The associated West-East displacement of the SHL is evident. For negative NAFDI, the Atlantic low-level cool northerly wind arriving to North Africa in the 10°-20º W stripe contributes also to cool the surface and keep the SHL in its East position (see Supplement S7). The anomalies of LLAT for positive and negative NAFDI confirm these results (see Supplement S8).

Once provided a physical explanation to the relationship between NAFDI and the SHL, we assess numerically the causality of this relationship computing the Pearson correlation coefficient with time lag between the daily SHLWEDI and the daily NAFDI for the 1980-2013 summer period (from 20 June to 17 September). Time-lag correlation coefficients are shown in Table 2. The maximum correlation coefficient (0.77) is obtained when the SHLWEDI is lagged one day after the NAFDI (Figure 10). This confirms numerically that NAFDI drives the SHL displacement. The correlation is even higher (0.80) if the correlation is performed between the daily SHLWEDI and 3-day backward-running-mean NAFDI since this account for the persistence in time of the driver. The simple visual inspection of Figure 10 indicates that the plotted points are asymmetrical distributed with a higher number of cases for both NAFDI and 1-day-lagged SHLWEDI positive values, and a larger variation range when both indexes are negative, thus confirming visually the findings detailed in the next paragraph.

Table 2. Pearson correlation coefficient with time lag between the daily SHLWEDI and the daily NAFDI for the summer period 20 June – 17 September and for the years 1980-2013. The column "Time lag" indicates the lag of the SHLWEDI after the NAFDI.

Time lag (days)	Pearson Correlation
3	0.550
2	0.704
1	**0.770**
0	0.688
-1	0.497

We have calculated the frequency distribution of the daily SHLWEDI and the NAFDI. For the NAFDI, the mean is 0.118 and the standard deviation 2.67, whereas for the SHLWEDI, the mean is 0.131 and the standard deviation 3.15. The index means are slightly larger than zero instead of being equal to zero because of the application of a 29-day running mean to the reference averages (see equations 1 and 2, respectively). We have observed that the SHL West-phase (positive NAFDI) is significantly more frequent than the SHL East-phase (negative NAFDI), especially for values of the index significantly different from zero (e.g., a

Atmos. Chem. Phys. Discuss., doi:10.5194/acp-2016-287, 2016
Manuscript under review for journal Atmos. Chem. Phys.
Published: 22 April 2016

departure from zero larger than a half of the standard deviation), as the statistics summary of the frequency distribution of the daily SHLWEDI and NAFDI shows in Table 3. This implies that the SHL East-phase (negative NAFDI) is usually more intense in absolute value (but less frequent) than the SHL West-phase (positive NAFDI), since the indexes have been defined using anomalies. Note that the frequencies of both indexes are very similar to each other, thus confirming the close relationship between them.

Table 3. Probability to have a value for the index (daily SHLWEDI or NAFDI) meeting the indicated condition (first column) for the reference period 1981-2010, 20 June – 17 September. For the SHLWEDI, the Index Mean=0.131 and standard deviation= 3.15; whereas for the NAFDI, the Index Mean=0.118 and Sigma=2.67.

Condition on the Index	**SHLWEDI**	**NAFDI**
< – Sigma/2	25.5%	26.2%
< Index Mean – Sigma/2	26.5%	27.0%
<0	43.0%	43.2%
< Index Mean	44.4%	45.4%
> 0	57.0%	56.9%
> Index Mean	55.6%	54.6%
> Sigma/2	35.3%	34.6%
> Index Mean + Sigma/2	33.5%	32.7%

We have found that the SHLWEDI values associated to the East-phase (negative NAFDI) are usually larger in absolute value (but less frequent) than those SHLWEDI values associated to the West-phase (positive NAFDI). This seems to be contradictory with the findings of Lavaysse et al. (2010a), that is, just the opposite. We think the Lavaysse et al. (2010a) statistics might be slightly biased because: 1) they selected a domain where the occurrence probability of the SHL cumulated over the period they considered exceeds 75%; 2) days when the centre of the SHL was not located in that area were discarded; 3) they used the same definition of SHL centre as Lavaysse et al. (2009), according to which (see their Fig. 8-b), the

Atmos. Chem. Phys. Discuss., doi:10.5194/acp-2016-287, 2016
Manuscript under review for journal Atmos. Chem. Phys.
Published: 22 April 2016

centre of the SHL is indeed located on the East side of the region with maximum WAHL occurrence frequency, minimum geopotential height, and containing the centre of the SHL cyclonic circulation. All these facts together suggest that, likely, a higher number of days with East SHL displacement than days with West SHL displacement were discarded by Lavaysse et al. (2010a). In the Supplement S9 we present statistics that point out that the SHL is indeed more intense during its East-phase, using a definition of intensity equivalent to that of Lavaysse et al. (2010a). Note that this does not imply necessarily that the SHL in its West position is weaker (according to its effect in the surrounding geographical area) than in its East position, but that the concept of SHL intensity does need to be revised and improved. We present latter in this subsection new ideas concerning the concept of SHL intensity and propose an improved definition for it.

A dipolar structure associated to the SHL position appears markedly when we correlate monthly values of NAFDI with NCEP-NCAR Renalysis 850 hPa Omega fields for the period 1980-2013 in July and August (Figure 11). A positive NAFDI (West SHL phase) produces a negative Omega anomaly on the West and a positive Omega anomaly on the East. This is probably due to the displacement of the SHL and its associated centre of net upward air transport (i.e., the forced secondary circulation associated to boundary layer pumping; e.g., see Holton, 1992), likely being produced the latter through a vertical imbalance in the thermal convection mass transport.

The onset of the SHL (and associated few-day delayed West African Monsoon onset; see Lavaysee et al. (2009) for the definition of these terms) might likely be triggered when the CBL achieves enough depth in the WAHL. This probably allows an increase and very efficient maintenance of the WAHL secondary circulation (convergence in the lower level low and divergence in the upper level high) that would increase the intensity of the thermal low, and therefore the intensity of the associated low-level cyclonic circulation (and probably also the monsoon wind intensity). Lavaysee et al. (2009) found that just after the SHL onset, the WAHL detection threshold decreases suddenly. We suggest the following explanation: the secondary circulation increases suddenly just after the SHL onset; this secondary circulation transports very efficiently air and heat (by advection) toward the centre of the SHL where they are lifted up till around 700 hPa, and then transported toward the Atlantic or Mediterranean. This mechanism cools a bit the surrounding area of the SHL, hence decreasing the WAHL detection threshold.

Lavaysse et al. (2010a) and Lavaysee et al. (2015) use the low-level atmospheric thickness as a proxy for the intensity of the SHL. However, we think the absolute thickness has not all the information concerning the intensity of the SHL. Northern Africa in summer has a mean surface air temperature higher in its central part than in its western part. This fact may lead systematically to higher low-level atmospheric thickness during the SHL East-phase. On the other hand, the SHL is a thermal low, and what defines a thermal low is the increase in temperature (and resulting: relative minimum in surface pressure and low-level cyclonic circulation) relative to the temperature of the surrounding geographical area. Therefore, we think the concept of SHL intensity might be significantly improved by defining the SHL intensity as the difference between the mean value of the low-level geopotential thickness within the SHL and the mean value of this field around the SHL area.

We know that dust sources in the Sahara region coincide with endorheic basins, of which there is a great number in this vast region (Ashpole and Washington, 2013; Ginoux et al., 2012). These dust sources are largely activated by low-level jets (LLJs) embedded in both the Harmattan flow and the south-westerly West African monsoon (WAM) flow (Allen et al., 2013; Fiedler et al., 2013; Marsham et al., 2013; Cowie et al., 2104). These flows are, in turn, modulated by the SHL displacements and intensity changes (i.e. Lavaysee et al., 2010; Couvreux et al., 2010), which are modulated by the NAFDI variations as we have seen.

The AOD anomalies plots show that under negative NAFDI (SHL East-phase), a significant increase of dust all over the Sahara is observed, except in the westernmost part, with a maximum in large part of Algeria and the Sahel belt (Figure 2), while the opposite happens with positive NAFDI. Wind anomaly maps at 925 hPa (Supplement S7) indicate that there is a significant W-SW axis anomaly in southern and central Algeria during negative NAFDI, which closely resembles the wind anomaly found by Ashpole and Washington (2013) precisely in the scenario referred to as HIGHDUST. This anomaly means a weakening and retraction of the Harmattan and a strengthened West African monsoon (WAM) inflow. On the contrary, we find strong positive AOD anomalies over the CWS hot spot (centred around 19°N, 5°W) analyzed by Knippertz et al. (2010) during positive NAFDI (SHL West-phase).

Focusing on specific dust source areas, Ashpole and Washington (2013) performed a thorough analysis in two regions of the CWS: the Mali-Algeria-Niger border triple-point (TP) and the Mali-Algeria border (MAB). They found that when dust occurs near the TP, the SHL tends to be located in central/southern Algeria (East-Phase of the SHL) while when dust is in

Atmos. Chem. Phys. Discuss., doi:10.5194/acp-2016-287, 2016
Manuscript under review for journal Atmos. Chem. Phys.
Published: 22 April 2016

the MAB region the SHL shows a strong preference for being located in western-most Algeria, northwest Mali, and northern Mauritania (SHL West-phase). This is exactly what we find: higher AOD in MAB for positive NAFDI (SHL West-Phase), what agrees Rodríguez et al. (2015) who reported significant dust activation in the region referred to as Subtropical Saharan Stripe (SSS) under positive NAFDI, and much higher AOD in TP during negative NAFDI (SHL East-Phase). In order to confirm the latter, we have calculated the AOD monthly averages for the August months of the period 2003-2012 in a region centred in the TP (5°W-15°E, 15°-25°N) that covers northern Mali, the southern third of Algeria, and northern Niger. We observe, from two independent satellite sensors (MODIS and MISR) data sets (Figure 12), that years with more negative NAFDI values show increased AOD, while the opposite occurs for months with more positive NAFDI values.

According to Roehrig et al. (2011), during SHL East-phase events (negative NAFDI) the eastern part of the SHL is intensified favouring convection reinforcement over Chad and Sudan. The MODIS AOD anomalies (Figure 2) indicate a clear AOD increase in these regions of eastern Sahel during negative NAFDI for June and July, although not in August.

The generally good agreement with previous results in the literature indicates that changes in NAFDI also modulate largely the activation / deactivation of dust sources in the central Sahara, and not just dust transport at regional-synoptic scale.

3.4 Relationship between NAFDI and Rossby waves

Roehrig et al. (2011) reported that the Azores anticyclone is largely impacted by the passage of a Rossby wave during the East-phase of the SHL, relating the changes of the structure of the Azores anticyclone with the enhanced (weakened) ventilation they observed during the SHL East-phase (West-phase), as indicated in section 3.3. However, these authors did not enter to explain the causal relationship between Rossby waves and phase changes of the SHL.

Chauvin et al. (2010) performed an EOF analysis of the NCEP2 850-hPa potential temperature in a rectangular domain containing part of North Africa. The first EOF they obtained (28% of the variance) resembles SAL intrusions into the Atlantic and Mediterranean, though they did not mention this explicitly since they focused on the SHL modes of intra-seasonal variability. Then, they performed a Complex EOF analysis and used the first eigenvalue to construct time-lag composites of the 1979-2007 NCEP meteorological fields as follows: 1) they identified 113 (115) significant maxima of the West- (East-) phase for this period; 2) for each phase they computed mean fields (for the days of maximum phase, and for several time lags respect to the days of maximum phase); 3) finally, they computed and plotted composite fields consisting in the difference of the two phase fields (West-phase minus East-phase), for the different time lags. Figures 5 and 7 from Chauvin et al. (2010) are particularly relevant for the present work, since they show the composite fields for horizontal wind vector, at both 850 hPa and 200 hPa, as well as potential temperature for 850 hPa and geopotential height for 200 hPa, from lag minus 6 days till plus 4 days. They indicated the observed pattern showed a clear Rossby wave signature.

We add the following comments to the interesting results of Chauvin et al. (2010). The Rossby wave pattern shown by them, in fact, represents the difference of a Rossby wave and the same Rossby wave after applying to it a pi-radian phase shift. Moreover, the wind patterns at 850 and 200 hPa are quite similar each other. This suggests the Rossby wave is barotropic. Those figures what show, in fact, is a Rossby wave packet that propagates from West to East with a group velocity much larger than its phase velocity. This is typical of barotropic free Rossby waves with the meridional and longitudinal wave numbers that the carrier of this wave packet has (e.g., Holton, 1992).

According to Chauvin et al. (2010) the arrival to Southern-Western Europe of Rossby waves propagating along the Northern Hemisphere upper troposphere waveguide drives, somehow, the phases of the SHL. In the previous subsection, we have shown that the NAFDI drives the SHL phases, and that the NAFDI is driven by variations in the lower-troposphere wind field at synoptic scale. Here, we show that these synoptic variations are driven by the arrival of mid-latitude free barotropic Rossby waves, through the upper troposphere, that impose its dynamical structure (perturbed wind and geopotential fields) as a perturbation that is added to the state of the lower troposphere. However, the influence of a free barotropic Rossby wave will not only depend on its amplitude in the upper troposphere but also on its capacity to go deep into the lower troposphere. An essential feature of the atmosphere at the considered latitudes and altitudes is the dependence on height of the zonal flow (thermal wind). This will affect the free barotropic Rossby waves since their local phase speed and group velocity depend on the zonal flow velocity. Therefore, the resulting differential advection of vorticity in the different pressure levels (due to the fact that the local phase speed is different for each level) will produce vertical motions that will keep the quasi-geostrophic balance (e.g., Holton, 1992).

Geisler and Dickinson (1975) considered a vertically isothermal atmosphere with a realistic vertical wind shear, and computed external Rossby modes (these are the equivalent to the free barotropic Rossby waves that hold for an atmosphere with no vertical wind shear). In the Supplement S10 we provide some analytical relations, obtain an equation that describes the Omega field associated to this wave in terms of the Geisler and Dickinson eigenvector, and prove with NCEP time series there is an empirical relation between the Omega amplitude at 500 hPa (at 2.5° E and 32.5° N, Northeast Algeria) and the vertical shear of the zonal flow. Based on those results, we use the Omega at 500 hPa as a tracer of the capacity of the free barotropic Rossby wave to go deep in the lower troposphere. We select the 500 hPa level because it is between the lower and upper troposphere. Lower levels might be sensitive to the SHL feedback (unwanted effect) whereas higher levels might not be very sensitive to the vertical wind shear in the middle and lower troposphere. The selected geographical location corresponds to a relative maximum in the correlation (around 0.6) between omega at 500 hPa and the monthly NAFDI for August months of the period 1980-2013 (see Figure S11-8 of Supplement S11). Chauvin et al. (2010) pointed out the existence of an anomalous northeasterly subsidence in this region (see their Fig. 10b) associated to the Rossby wave, but they did not explain the origin and the implications of this subsidence anomaly. Note that the Geisler and Dickinson (1975) background zonal flow does not have latitudinal dependence, and therefore does not account for the latitudinal waveguide phenomenon. Accounting for both types of background dependences (in latitude and height) simultaneously (not done in the literature, according to our knowledge) will probably make the frequency spectrum of the Rossby wave eigenvectors much more complex and rich. For a particular vertical wind shear distribution, there might be also differences in the vertical distribution of the eigenvector amplitude depending on the frequency and the longitudinal wave-number of the eigenvector. These arguments are used latter in this section to interpret the power spectra of some time series.

We have computed NCEP monthly correlation and regression plots between the zonal (and meridional) wind at different pressure levels (all the NCEP reanalysis levels between 70 and 925 hPa) and the monthly NAFDI for August months of the period 1980-2013 (see Supplement S6). The wave pattern observed is very similar to that observed by Chauvin et al.

(2010) in a broad range of levels. The maximum correlation (between -0.8 and -0.9) in absolute value observed at the upper levels takes place for the zonal wind at 300 hPa, 10°W, 30°N. Using the corresponding regression plots, we have obtained at this point (or near neighbourhood, since there is a small tilt in the vertical direction) the amplitude of the wave at each pressure level, shown in Figure 13 For reference, the vertical distribution of the amplitude for pure free barotropic Rossby waves in an isothermal atmosphere with a uniform zonal flow (each function has been normalized relative to its maximum amplitude) is also shown in Figure 13 This figure indicates that the Rossby wave that drives the NAFDI variations goes deeper in the lower troposphere than the pure free barotropic Rossby wave. In the Supplement S12 we show that the vertical structure of the Rossby wave that drives the NAFDI variations is very similar to the vertical structure of the external Rossby wave of Geisler and Dickinson (1975) with "effective wavenumber" 10.8.

The vertical structure of an external Rossby wave is very sensitive to the actual vertical profile of the horizontal wind. Therefore, the impact of the Rossby wave on NAFDI variations should not only depend on the amplitude and phase of the Rossby wave at 200-300 hPa, but also on the penetration of the Rossby wave into the lower troposphere. To quantify the former we use the daily NCEP Zonal Wind Anomaly at 300 hPa over South Morocco (10°W and 30°N) multiplied by -1, denoted as ZWA300, whereas to quantify the latter we use the daily NCEP Omega at 500 hPa over Northwest Algeria (2.5° E, 32.5° N), denoted as O500. Note that we do not use the anomaly for Omega, but the full value. For the period 1980-2013 20 June – 17 September, the mean value of O500 is 0.00347 Pa s^{-1} (probably due to the subsident subtropical branch of the Hadley circulation) whereas the standard deviation is 0.0492 Pa s^{-1} (much larger than the mean value). However, ZWA300 is an anomaly respect to the 29-day-running-mean average daily value for the period of reference 1981-2010 (as in the daily NAFDI and SHLWEDI definitions).

Table 4 shows the Pearson correlation coefficient between the daily ZWA300, O500 and NAFDI (also for some time lags as well as 5-day running means). The results led to the following conclusions: 1) the correlation of both ZWA300 and O500 with NAFDI is significant; 2) the correlation between ZWA300 and O500 is low but not negligible (these two facts together indicate that ZWA300 and O500 are quasi-independent indexes that take into account different aspects of the Rossby wave in agreement with our previous discussion); 3) it seems that ZWA300 drives almost one day in advance the value of NAFDI, whereas O500

Atmos. Chem. Phys. Discuss., doi:10.5194/acp-2016-287, 2016
Manuscript under review for journal Atmos. Chem. Phys.
Published: 22 April 2016

might be ahead respect to NAFDI less than 12 hours, which agrees what is shown in Figures 5 and 7 of Chauvin et al. (2010): a Rossby wave-packet comes from the Northwest Atlantic and approaches Northern Africa days before a maximum in the SHL displacement is achieved, reaching the centre of the wave-packet Northern Africa when that maximum is achieved ; 4) when applying 5-day running means to the time series before computing the correlation coefficients, they increase significantly (because of the removal of part of the "noise" due to synoptic signal). When performing a multilinear least-square regression of daily NAFDI as function of ZWA300 and O500, a linear correlation of 0.533 is obtained (0.656 for 5-day running means). Supplement S13 provides more details about these regressions.

Table 4. Pearson correlation coefficient between the indicated daily time series (some of them lagged). "if 5drm" indicates that the correlation coefficient in case a 5-day running mean is applied to both daily time series.

Correlation between	ZWA300	O500
ZWA300		
O500	0.105 (if 5drm: 0.205)	
O500 lagged 1 day	0.159	
NAFDI lagged 1 day		0.309
NAFDI	0.363 (if 5drm: 0.483)	0.426 (if 5drm: 0.534)
NAFDI lagged 1 day	0.386	0.395
NAFDI lagged 2 days	0.342	

We have computed the power spectra of the daily NAFDI, SHLWEDI, ZWA300 and O500 time series for the period 20 June -17 September 1980-2013 using Fast Fourier Transform (e.g., Press et al., 1994), after padding with zeros till complete 4096 elements in each time series (i.e., the nearest larger power of 2). In Supplement S14, a plot of the NAFDI power spectrum is presented. The overall structure of the NAFDI, SHLWEDI, ZWA300 and O500 power spectra is quite similar (not shown). Grosso modo, the spectral power decreases as

Atmos. Chem. Phys. Discuss., doi:10.5194/acp-2016-287, 2016
Manuscript under review for journal Atmos. Chem. Phys.
Published: 22 April 2016

frequency increases, but there are peaks superposed to this trend. Supplement S14 also contains a table (Table S14) that shows the distribution of spectral power in the different frequency ranges. We consider the following ranges of time scales (and assign a name to each range): 1) long time scales (period larger than 30 days); 2) intermediate time scales (period between 10 and 30 days); 3) sub-intermediate time scales (period between 5 and 10 days); 4) short time scales (period smaller than 5 days).

The intermediate time scale range is considered as the range of the Rossby waves (e.g., Ambrizzi et al., 1995). The Rossby wave pattern identified by Chauvin et al. (2010) has a period of 15 days approximately, but the spectrum they obtained has signal in all the intermediate time scale range. We have reconstructed our 4 time series using only the Fourier components of the intermediate range (i.e., application of a band-pass filter), and computed the Pearson correlation between these filtered time series. The correlations are quite similar to those previously obtained for the no-filtered time series, except for NAFDI vs. O500 that have a correlation between them of 0.49 for the filtered daily time series whereas the correlation is 0.43 for the no-filtered daily time series. This rather high correlation (0.49) confirms that the influence of O500 on NAFDI operates in the time scales of the Rossby waves.

In Supplement S14, Figure S14-2, the power spectra of the 4 time series in the intermediate range are plotted, showing the following main facts: 1) the 10 more intense NAFDI spectral peaks have periods of 30.0, 27.7, 26.1, 23.7, 21.6, 18.1, 15.6, 15.1, 14.1 and 13.7 days, but there are many other spectral peaks (the spectrum shown by Chauvin et al. (2010) in their Figure 4 for their first eigenvalue of SHL variability, has a poorer resolution); 2) most of the intense peaks appear also in the SHLWEDI power spectrum; 3) for many of the NAFDI/SHLWEDI peaks, there is associated an O500 and/or ZWA300 peak. That is, the modes of oscillation of the NAFDI and the SHL are driven by mid-latitude Rossby waves of different characteristics. For example, a similar impact is produced by a Rossby wave very intense in the upper troposphere but that does not penetrate very deep in the lower troposphere, than by a Rossby wave not very strong in the upper troposphere but that penetrate very deep in the lower troposphere. Only those Rossby waves that impose a significant perturbation in the lower troposphere are able to drive the NAFDI, and consequently the SHL displacement.

In this study we do not address the modulation that mid-term and long-term climate oscillations might introduce on the interactions between Rossby waves, NAFDI, SHL and

Atmos. Chem. Phys. Discuss., doi:10.5194/acp-2016-287, 2016
Manuscript under review for journal Atmos. Chem. Phys.
Published: 22 April 2016

dust export, since it is out of the scope of the present paper. Long-term analysis (1950-2013) on relationships between Saharan dust export over the North Atlantic and the main climate indexes is tackled in the complementary study García et al. (2016).

4 Summary and conclusions. A comprehensive top-down atmospheric conceptual model: from hemispheric to meso-scale atmospheric mechanisms driving dust mobilization and transport over Northern Africa

In this study, we have revised and improved the definition of the NAFDI by selecting a new meridional point. This revision was motivated by the fact that the geopotential heights over the two regions used to define the former NAFDI correlate positively, and therefore, their variations are not completely independent. The "improved NAFDI" index shows a higher correlation range with the geopotential height at 700 hPa. Moreover, the geopotential height derivative anomaly that the improved NAFDI provides is calculated along a line that is perpendicular to the geostrophic wind anomaly and crosses the core of the SHL. As a result, the total dust concentrations measured at the Izaña Atmospheric Observatory in August months (from 1987 to 2014) and the NAFDI time series for that period show a better Pearson correlation coefficient between them when using the improved NAFDI (0.72 instead of the value 0.67 that is obtained when using the original NAFDI definition). The monthly NAFDI values for the period 1948-2015 are available at http://izana.aemet.es/dataseries/.

Three large patterns of MODIS AOD anomalies over dust transport regions out of northern Africa (North Atlantic and the Mediterranean) are found for each month and phase of the NAFDI. First, we observe a significant positive (negative) NE-SW axis AOD anomaly over the Subtropical North Atlantic for positive (negative) NAFDI. A second notable pattern is the positive (negative) AOD anomaly over the tropical Atlantic during negative (positive) NAFDI, and a third remarkable positive (negative) AOD anomaly pattern is found over Central-Western Mediterranean under negative (positive) NAFDI. When using MACC reanalysis, we obtain the same striking patterns of AOD anomalies, although remarkably smoothed. We highlight the fact that every summer we find months with both positive and negative NAFDI values, but the AOD-anomalies patterns found in the months with the same NAFDI phase are the same regardless of the considered month. This suggests that there are some well-defined dust-transport patterns on these regions, which are basically modulated by the NAFDI. As a secondary result we note that the fairly good agreement between MODIS and MACC reanalysis confirms the suitability of MACC for climatological studies, like the present one.

We have found outstanding similarities in the meteorological patterns associated with the positive NAFDI and the SHL West-phase, on the one hand, and with the negative NAFDI and SHL East-Phase, on the other hand, suggesting a close relationship between the NAFDI and the SHL. This relationship has been physically explained, and quantified in the present study. In order to assess this close relationship, we first introduced two new indexes: the daily NAFDI index (instead of monthly), and the daily SHL West-East Displacement Index (SHLWEDI). The Pearson correlation coefficient between the daily SHLWEDI and the daily NAFDI for the period 1980-2013 20 June – 17 September (there are 3,060 data pairs) is fairly high (0.69). Moreover, the correlation coefficient increases to 0.77 when the SHLWEDI is lagged one day after the NAFDI, and the correlation is maximized (0.80) when the correlation is performed between the daily SHLWEDI and the 3-day backward-running-mean NAFDI since this account for the persistence in time of the driver. The physical explanation to the relationship between the NAFDI and the SHL is summarized at the end of this section through a conceptual model.

We have found that the SHL West-phase is significantly more frequent than the SHL East-phase, implying that the SHL East-phase is usually more intense in absolute value, but less frequent, than the SHL West-phase. We have confirmed that the SHL is indeed more intense during its East-phase using a simplified definition of intensity equivalent to that of Lavaysse et al. (2010a). So, we think the concept of SHL intensity might be significantly improved by defining the SHL intensity as the difference between the mean value of the low-level geopotential thickness (700-925 hPa) within the SHL and the mean value of this field around the SHL area.

A dipolar structure associated to the SHL position appears markedly when we correlate monthly values of NAFDI with NCEP Reanalysis 850 hPa Omega fields for the period 1980-2013 in July and August. This is probably due to the displacement of the SHL and its associated centre of net upward air transport, likely being produced the latter through a vertical imbalance in the thermal convection mass transport.

Concerning the onset of the SHL, it might likely be triggered when the CBL achieves enough depth in the WAHL. This probably allows an enhancement and very efficient maintenance of the WAHL secondary circulation (convergence in the lower level low and divergence in the

Atmos. Chem. Phys. Discuss., doi:10.5194/acp-2016-287, 2016
Manuscript under review for journal Atmos. Chem. Phys.
Published: 22 April 2016

upper level high) that would increase the intensity of the thermal low, and therefore the intensity of the associated low-level cyclonic circulation, and probably also the monsoon wind intensity. The increase of the secondary circulation just after the onset of the SHL might act as cooling mechanism of the surrounding area of the SHL, decreasing then the WAHL detection threshold.

Positive AOD anomalies in the west Sahara during positive NAFDI / SHL West-phase, and positive AOD anomalies in the central and eastern Sahara during negative NAFDI / SHL East-phase, have been found. This is consistent with the fact that a large part of the mesoscale baroclinic mechanisms that produce dust mobilization are associated with SHL displacements and intensity changes. Thus, it seems that NAFDI also modulates largely the activation / deactivation of dust sources in the Sahara, and not just the dust transport out of northern Africa at regional-synoptic scale.

We have found that the NAFDI is driven by variations in the lower-troposphere wind field at synoptic scale, which is driven, in turn, by the arrival of mid-latitude free barotropic Rossby waves that impose their perturbed wind and geopotential fields to the state of the lower troposphere. The impact of a Rossby wave on NAFDI variations depends on both the amplitude and phase of the Rossby wave at 200-300 hPa, which is quantified in this study by the daily NCEP Zonal Wind Anomaly at 300 hPa over South Morocco (10°W and 30°N) (ZWA300), and the penetration of the Rossby wave into the lower troposphere, quantified by the daily NCEP Omega at 500 hPa over Northwest Algeria (2.5° E, 32.5° N) (O500). We have proved that there is an empirical relation between the Omega amplitude at 500 hPa and the vertical shear of the zonal flow. The correlation of both ZWA300 and O500 with NAFDI is significant: 0.48 and 0.53, respectively, when we apply a 5-day running mean to the time series before calculating the correlation coefficients, and the correlation increases to 0.66 when performing a multi-linear regression. These numbers remain large when a 10-30 day band-pass filter is applied to the time series. The results suggest that ZWA300 drives almost one day in advance the value of NAFDI, whereas O500 might be ahead respect to NAFDI less than 12 hours.

We have computed the power spectra of the daily NAFDI, SHLWEDI, ZWA300 and O500 time series for the period 20 June -17 September 1980-2013 using Fast Fourier Transform. The NAFDI power spectrum shows in the intermediate time scale range (between 10 and 30 days; considered as the time scale range of the Rossby waves) 10 intense spectral peaks with

Atmos. Chem. Phys. Discuss., doi:10.5194/acp-2016-287, 2016
Manuscript under review for journal Atmos. Chem. Phys.
Published: 22 April 2016

Atmospheric Chemistry and Physics
Open Access
Discussions

centres ranging from 13.7 to 30 days (additionally to other less intense peaks). Most of these intense peaks also appear in the SHLWEDI spectrum, and for many of the NAFDI/SHLWEDI peaks there is associated an O500 and/or ZWA300 peak. These results indicate that the modes of oscillation of both the NAFDI and the SHL are driven by mid-latitudes Rossby waves propagating through the North Atlantic and North African waveguide, but only those Rossby waves that go deep enough into the lower troposphere to impose their structure as a significant perturbation superposed to the background.

The close physical interactions between mid-latitude Rossby waves, NAFDI and SHL phases, and their impact on dust mobilization in the Sahara and its transport out of Africa, are briefly summarized in the following comprehensive top-down conceptual model, which is schematized in Figure 14.

1. Here we start the sequence assuming an initial positive NAFDI (SHL West-phase) in which the North African high at 700 hPa transports hot air from above the SHL towards the subtropical North Atlantic. The Azores and North African highs at 700 hPa are very close each other. The intense ageostrophic wind component at 700 hPa (this level is within the CBL) allows upper SAL air masses arrive till the region of influence of the Azores high, which transports dust-laden air masses westwards over the North Atlantic. The advection of hot Saharan air across the subtropical North Atlantic also contributes to increase the geopotential thickness of the region located between the Azores and North Africa highs, merging them into an apparent single 700 hPa anticyclone extended across much of the North Atlantic and North Africa. During positive NAFDI (SHL West-phase) we observe strong positive AOD anomalies over the CWS hot spot (centred around 19°N, 5°W) and on the Subtropical Saharan Stripe. This is consistent with a more intense low-level cyclonic circulation in Western Sahara associated to the SHL in its West-phase.

2. When a free barotropic Rossby wave propagating through the North Atlantic and North African waveguide produces an intense enough Northerly wind component in the upper troposphere over the subtropical 10-20º W stripe, and the structure of this Rossby perturbation goes deep enough into the lower troposphere, we find advection of colder air from northern latitudes into the subtropical 10-20º W stripe lower troposphere, what results in a negative advection of geopotential thickness, causing a NE-SW axis through in the 700 hPa geopotential height which separates the Azores and North African highs at 700 hPa experiencing the latter a slightly eastward shift. At the same time, the Rossby wave imposes a

positive zonal wind anomaly over Northern Africa, advecting the mid-level SAL toward the East. This shift toward the East favours heating over the easternmost position of the SHL, causing its eastward shift around one day later. The persistence of the NE-SW axis through in the whole troposphere and the subsequent displacement of the SHL to the East contribute also to cool the surface in the western part and keep the SHL in its East position. Under negative NAFDI (SHL East-phase) we find a significant increase of dust over the Sahara, except in its westernmost part where we observe negative AOD anomalies, with a maximum in large part of Algeria and the Sahel belt. Much higher AOD in the Mali-Algeria-Niger border is found in this scenario, and dust is transported into the Western-central Mediterranean.

3. When a free barotropic Rossby wave produces an intense enough Southerly wind component in the upper troposphere over the subtropical 10-20º W stripe, and the structure of this Rossby perturbation goes deep enough into the lower troposphere decreasing substantially the strong meridional flow of cold air present in the lower troposphere (due to the East branch of the Azores high) the deep through is considerably weakened. At the same time, the Rossby wave imposes a negative zonal wind anomaly over Northern Africa, advecting the mid-level SAL toward the West. The North African high at 700 hPa shifts back to its westernmost position starting the cycle again.

In summary, we have demonstrated that the SHL position is modulated by the NAFDI, and that the latter is modulated by mid-latitude Rossby waves. The phases of the NAFDI and the SHL drive dust mobilization in different parts of the Sahara and define the transport of mineral dust outside Africa through certain prevalent pathways.

Acknowledgements

This study has been developed within the activities of the WMO Sand and Dust Storm Warning Advisory and Assessment System (SDS WAS) Regional Centre for Northern Africa, Middle East and Europe, hosted by the State Meteorological Agency of Spain (AEMET) and the Barcelona Supercomputing Centre (BSC-CNS). This work is also a contribution to Copernicus CAMS-84. The authors wish to thank ECMWF for providing ERA-Interim data and MACC-dust reanalysis. Our acknowledgment to NCEP/NCAR Reanalysis Project at the NOAA/ESRL Physical Sciences Division. Satellite data used in this work were obtained through NASA LADS ftp server (ladsweb.nascom.nasa.gov/allData/6/) and Giovanni web server belongs to Goddard Earth Sciences, Data and Information Services Center (GES-DISC;

Atmos. Chem. Phys. Discuss., doi:10.5194/acp-2016-287, 2016
Manuscript under review for journal Atmos. Chem. Phys.
Published: 22 April 2016

http://disc.sci.gsfc.nasa.gov/giovanni). A.J. Gomez-Pelaez acknowledges the PhD Programme "Physics and Space Sciences" of the University of Granada (Spain), in which he is enrolled. Part of this study was performed in the frame of AEROATLAN (grant 2015-66229), funded by the Ministry of Economy and Competitiveness of Spain.

References

Adams, A. M., Prospero, J. M., and Zhang, C.: CALIPSO derived three-dimensional structure of aerosol over the Atlantic Basin and adjacent continents, J. Climate, 25, 6862–6879, doi:10.1175/JCLI-D-11-00672.1, 2012.

Allen, C. J. T. and Washington, R.: The low-level jet dust emission mechanism in the central Sahara: Observations from Bordj-Badji Mokhtar during the June 2011 Fennec Intensive Observation Period, J. Geophys. Res. Atmos., 119, 2990–3015, doi:10.1002/2013JD020594, 2013.

Alonso-Pérez, S., Cuevas, E., Querol, X., Viana, M., Guerra, J.C.: Impact of the Saharan dust outbreaks on the ambient levels of total suspended particles (TSP) in the Marine Boundary Layer (MBL) of the Subtropical Eastern North Atlantic Ocean, Atmospheric Environment, 41/40, 9468-9480. DOI: 10.1016, 2007.

Ambrizzi, T., Hoskins, B. J., and Hsu, H. H.: Rossby-wave propagation and teleconnection patterns in the austral winter, Journal of the Atmospheric Sciences, 52, 3661-3672, 1995.

Ashpole, I. and Washington, R.: Intraseasonal variability and atmospheric controls on daily dust occurrence frequency over the central and western Sahara during the boreal summer, J. Geophys. Res.-Atmos., 118, 12915–12926, doi:10.1002/2013JD020267, 2013.

Basart, S., Pérez C., Cuevas E., Baldasano J.M., Gobbi G.P.: Aerosol characterization in Northern Africa, Northeastern Atlantic, Mediterranean Basin and Middle East from direct-sun AERONET observations. Atmos. Chem. Phys., 9, 8265-8282, 2009.

Bellouin, N., Quaas, J., Morcrette, J.-J., and Boucher, O.: Estimates of aerosol radiative forcing from the MACC re-analysis, Atmos. Chem. Phys., 13, 2045–2062, doi:10.5194/acp-13-2045-2013, 2013.

Ben-Ami, Y., Koren, I., and Altaratz, O.: Patterns of North African dust transport over the Atlantic: winter vs. summer, based on CALIPSO first year data, Atmos. Chem. Phys., 9, 7867–7875, doi:10.5194/acp-9-7867-2009, 2009.

Benedetti, A., Morcrette, J.-J., Boucher, O., Dethof, A., Engelen, R. J., Fisher, M., Flentjes, H., Huneeus, N., Jones, L., Kaiser, J. W., Kinne, S., Mangold, A., Razinger, M., Simmons, A. J., Suttie, M., and the GEMS-AER team: Aerosol analysis and forecast in the ECMWF

Integrated Forecast System. Part II: Data assimilation, J. Geophys. Res., 114, D13205, doi:10.1029/2008JD011115, 2009.

Bou Karam, D., Flamant, C., Knippertz, P., Reitebuch, O., Pelon, J., Chong, M., and Dabas, A.: Dust emissions over the Sahel associated with the West African monsoon intertropical discontinuity region: A representative case-study, Quart. J. Roy. Meteor. Soc., 134, 621–634, doi:10.1002/qj.244, 2008.

Boucher, O., Pham, M., and Venkataraman, C.: Simulation of the Atmospheric Sulfur Cycle in the LMD GCM: Model Description, Model Evaluation, and Global and European Budgets, Inst. Pierre-Simon Laplace, Paris, France, Note 23, 26 pp., available at: www.ipsl.jussieu.fr/poles/Modelisation/NotesSciences. htm (last access: 22 October 2014), 2002.

Canut, G., Lothon, M., Saïd, F., and Lohou, F.: Observation of entrainment at the interface between monsoon flow and the Saharan Air Layer, Q. J. Roy. Meteorol. Soc., 136, 34–46, 2010.

Cesnulyte, V., Lindfors, A. V., Pitkänen, M. R. A., Lehtinen, K. E. J., Morcrette, J.-J., and Arola, A.: Comparing ECMWF AOD with AERONET observations at visible and UV wavelengths, Atmos. Chem. Phys., 14, 593–608, doi:10.5194/acp-14-593-2014, 2014.

Chaboureau, J.-P., Flamant, C., Dauhut, T., Kocha, C., Lafore, J.-P., Lavaysse, C., Marnas, F., Mokhtari, M., Pelon, J., Reinares Martínez, I., Schepanski, K., and Tulet, P.: Fennec dust forecast intercomparison over the Sahara in June 2011, Atmos. Chem. Phys. Discuss., doi:10.5194/acp-2016-12, in review, 2016.

Charney, J. G., and Eliassen, A.: A numerical method for predicting the perturbations of the middle latitude westerlies, Tellus, 1, 38-54, 1949.

Chauvin, F., Roehrig, R., and Lafore, J.-P.: Intraseasonal variability of the Saharan heat low and its link with midlatitudes, J. Climate, 23, 2544–2561, doi:10.1175/2010JCLI3093.1, 2010.

Chen, T.-C.: Maintenance of the midtropospheric North African summer circulation: Saharan high and African easterly jet. J. Climate., 18, 2943 – 2962, 2005.

Chiapello, I., Moulin, C., and Prospero, J. M.: Understanding the long-term variability of African dust transport across the Atlantic as recorded in both Barbados surface concentrations

Atmos. Chem. Phys. Discuss., doi:10.5194/acp-2016-287, 2016
Manuscript under review for journal Atmos. Chem. Phys.
Published: 22 April 2016

and large-scale Total Ozone Mapping Spectrometer (TOMS) optical thickness, J. Geophys. Res., 110, D18S10, doi:10.1029/2004JD005132, 2005.

Couvreux, F., Guichard, F., Bock, O., Campistron, B., Lafore, J.-P., and Redelsperger, J.-L.: Synoptic variability of the monsoon flux over West Africa prior to the onset, Q. J. R. Meteorol. Soc., 136(S1), 159–173, doi:10.1002/qj.473, 2010.

Cuesta, J., Marsham, J. H., Parker, D. J., and Flamant, C.: Dynamical mechanisms controlling the vertical redistribution of dust and the thermodynamic structure of the West Saharan atmospheric boundary layer during summer, Atmos. Sci. Lett., 10, 34–42, doi:10.1002/asl.207, 2009.

Cuevas, E., Camino, C., Benedetti, A., Basart, S., Terradellas, E., Baldasano, J. M., Morcrette, J. J., Marticorena, B., Goloub, P., Mortier, A., Berjón, A., Hernández, Y., Gil-Ojeda, M., and Schulz, M.: The MACC-II 2007–2008 reanalysis: atmospheric dust evaluation and characterization over northern Africa and the Middle East, Atmos. Chem. Phys., 15, 3991-4024, doi:10.5194/acp-15-3991-2015, 2015.

Dee, D.P., Uppala, S.M., Simmons, A.J., Berrisford, P., Poli, P., Kobayashi. S., Andrae, U., Balmaseda, M.A, Balsamo, G., Bauer, P., Bechtold, P., Beljaars, A.C.M., van de Berg, L., Bidlot, J., Bormann, N., Delsol, C., Dragani, R., Fuentes, M., Geer, A.J., Haimberger, L., Healy, S.B., Hersbach, H., Hólm, E.V., Isaksen, L., Kållberg, P., Köhler, M., Matricardi, M., McNally, A.P., Monge-Sanz, B.M., Morcrette, J-J., Park, B-K., Peubey, C., de Rosnay, P., Tavolato, C., Thepaut, J-N., Vitart, F.: The ERA-Interim reanalysis: configuration and performance of the data assimilation system, Q. J. R. Meteorol. Soc. 137: 553–597. DOI:10.1002/qj.828, 2011.

Draxler, R. R. and Hess, G. D.: An overview of the HYSPLIT_4 modelling system for trajectories, dispersion, and deposition, Aust. Meteorol. Mag., 47, 295–308, 1998.

Engelstaedter, S. and Washington, R.: Atmospheric controls on the annual cycle of North African dust, J. Geophys. Res., 112, D17111, doi:10.1029/2006JD007195, 2007.

Escudero, M., Querol, X., Ávila A., and Cuevas, E.: Origin of the exceedances of the European daily PM limit value in regional background áreas of Spain, Atmos. Environ., 41, 730–744, 2007a.

Escudero, M., Querol, X., Pey, J., Alastuey, A., Pérez, N., Ferreira, F., Alonso, S., Rodríguez, S., and Cuevas, E.: A methodology for the quantification of the net African dust load in air quality monitoring networks, Atmos. Environ., 41, 5516–5524, 2007b.

Eskes, H. J., Benedictow, A., Blechschmidt, A.-M., Bouarar, I., Botek, E., Chabrillat, S., Christophe, Y., Cuevas, E., Clark, H., Flentje, H., Gaudel, A., Griesfeller, J., Huijnen, V., Huneeus, N., Jones, L., Kapsomenakis, J., Katragkou, E., Kinne, S., Langerock, B., Lefever, K., Melas, D., Razinger, M., Richter, A., Schulz, M., Thomas, W., Thouret, V., Vrekoussis, M., Wagner, A., and Zerefos, C.: Validation Report of the MACC Reanalysis of Global Atmospheric Composition: Period 2003– 2012, MACC Report, 29 June 2014, available at: http:// www.copernicus-atmosphere.eu/ (last access: 8 March 2016), 2014.

Eskes, H., Huijnen, V., Arola, A., Benedictow, A., Blechschmidt, A.-M., Botek, E., Boucher, O., Bouarar, I., Chabrillat, S., Cuevas, E., Engelen, R., Flentje, H., Gaudel, A., Griesfeller, J., Jones, L., Kapsomenakis, J., Katragkou, E., Kinne, S., Langerock, B., Razinger, M., Richter, A., Schultz, M., Schulz, M., Sudarchikova, N., Thouret, V., Vrekoussis, M., Wagner, A., and Zerefos, C.: Validation of reactive gases and aerosols in the MACC global analysis and forecast system, Geosci. Model Dev., 8, 3523-3543, doi:10.5194/gmd-8-3523-2015, 2015.

Fiedler, S., Schepanski, K., Heinold, B., Knippertz, P., and Tegen, I.: Climatology of nocturnal lowlevel jets over North Africa and implications for modeling mineral dust emission, J. Geophys. Res.-Atmos., 118, 6100–6121, doi:10.1002/jgrd.50394, 2013.

Flamant, C., J.-P. Chaboureau, D. J. Parker and C. M. Taylor: Airborne observations of the impact of a convective system on the planetary boundary layer thermodynamics and aerosol distribution in the inter-tropical discontinuity region of the West African Monsoon, Q. J. R. Meteorol. Soc. 10.1002/qj.97, 133, 626, 1175 – 1189, 2007.

Gallisai, R., Peters, F., Basart, S., and Baldasano, J. M.: Mediterranean basin-wide correlations between Saharan dust deposition and ocean chlorophyll concentration, Biogeosciences Discuss., 9, 8611–8639, doi:10.5194/bgd-9-8611-2012, 2012.

García, O.E., García, R.D., Cuevas, E., Gómez-Peláez, A.J., and Rodríguez, S.: Long-term (1950-2013) analysis of Saharan dust outbreaks over the subtropical North Atlantic, Geophys. Res. Lett., Submitted, 2016.

Geisler, J. E., and Dickinson, R. E.: External Rossby modes on a beta-plane with realistic vertical wind shear, Journal of the Atmospheric Sciences, 32, 2082-2093, 1975.

Gerasopoulos, E., Kouvarakis, G., Babasakalis, P., Vrekoussis, M., Putaud, J. P., and Mihalopoulos, N.: Origin and variability of particulate matter (PM10) mass concentrations over the Eastern Mediterranean, Atmos. Environ., 40, 4679–4690, 2006.

Ginoux, P., Prospero, J. M., Torres, O., and Chin, M.: Long-term simulation of global dust distribution with the GOCART model: Correlation with North Atlantic Oscillation, Environ. Modell. Softw., 19, 113–128, 2004.

Ginoux, P., Prospero, J. M., Gill, T. E., Hsu, N. C., and Zhao, M.: Global-scale attribution of anthropogenic and natural dust sources and their emission rates based on MODIS Deep Blue aerosol products, Rev. Geophys., 50, RG3005, doi:10.1029/2012RG000388, 2012.

Gkikas, A., Houssos, E.E., Lolis, C.J., Bartzokas, A., Mihalopoulos, N., Hatzianastassiou, N.: Atmospheric circulation evolution related to desert dust episodes over the Mediterranean, Quarterly Journal of the Royal Meteorological Society, 141, 690, 1634-1645, 2015.

Guerzoni, S., Chester, R., Dulac, F., Herut, B., Loye-Pilot, M.-D., Measures, C., Migon, C., Molinaroli, E., Moulin, C., Rossini, P., Saydam, C., Soudine, A., and Ziveri, P.: The role of atmospheric deposition in the biogeochemistry of the Mediterranean Sea, Prog. Oceanogr., 44, 147–190, 1999.

Guirado, C., Cuevas, E., Cachorro, V.E., Toledano, C., Alonso-Pérez, S., Bustos, J.J., Basart, S., Romero, P.M., Camino, C., Mimouni, C., Zeudmi, L., Goloub, P., Baldasano, J.M., and de Frutos, A. M., Aerosol characterization at the Saharan AERONET site Tamanrasset, Atmos. Chem. Phys. Discuss, acp-2014-252, 2014.

Haywood, J. M., Pelon, J., Formenti, P., Bharmal, N., Brooks, M., Capes, G., Chazette, P., Chou, C., Christopher, S., Coe, H., Cuesta, J., Derimian, Y., Desboeufs, K., Greed, G., Harrison, M., Heese, B., Highwood, E. J., Johnson, B., Mallet, M., Marticorena, B., Marsham, J., Milton, S., Myhre, G., Osborne, S. R., Parker, D. J., Rajot, J. L., Schulz, M., Slingo, A., Tanré, D., and Tulet, P.: Overview of the dust and biomassburning experiment and African monsoon multidisciplinary analysis special observing period-0, J. Geophys. Res., 113, D00C17, doi:10.1029/2008JD010077, 2008.

Holton, J. R.: An introduction to dynamic meteorology, Third edition, International Geophysics Series, vol. 48, Academic Press, San Diego, California, 1992.

Hoskins, B. J., and Ambrizzi, T.: Rossby-wave propagation on a realistic longitudinally varying flow, Journal of the Atmospheric Sciences, 50, 1661-1671, 1993.

Hoskins, B. J., and Karoly, D. J.: The steady linear response of a spherical atmosphere to thermal and orographic forcing, Journal of the Atmospheric Sciences, 38, 1179-1196, 1981.

Hsu, H. H., and Lin, S. H.: Global teleconnections in the 250-mb streamfunction field during the northern-hemisphere winter, Monthly Weather Review, 120, 1169-1190, 1992.

Hsu, N. C., Jeong, M.-J., Bettenhausen, C., Sayer, A.M., Hansell, R., Seftor, C. S., Huang, J., and Tsay, S.-C.:Enhanced Deep Blue aerosol retrieval algorithm: The second generation, J. Geophys. Res. Atmos., 118, 9296–9315, doi:10.1002/jgrd.50712, 2013.

Huneeus, N., Schulz, M., Balkanski, Y., Griesfeller, J., Prospero, J., Kinne, S., Bauer, S., Boucher, O., Chin, M., Dentener, F., Diehl, T., Easter, R., Fillmore, D., Ghan, S., Ginoux, P., Grini, A., Horowitz, L., Koch, D., Krol, M. C., Landing, W., Liu, X., Mahowald, N., Miller, R., Morcrette, J.-J., Myhre, G., Penner, J., Perlwitz, J., Stier, P., Takemura, T., and Zender, C. S.: Global dust model intercomparison in AeroCom phase I, Atmos. Chem. Phys., 11, 7781–7816, doi:10.5194/acp-11-7781-2011, 2011.

Inness, A., Baier, F., Benedetti, A., Bouarar, I., Chabrillat, S., Clark, H., Clerbaux, C., Coheur, P., Engelen, R. J., Errera, Q., Flemming, J., George, M., Granier, C., Hadji-Lazaro, J., Huijnen, V., Hurtmans, D., Jones, L., Kaiser, J. W., Kapsomenakis, J., Lefever, K., Leitão, J., Razinger, M., Richter, A., Schultz, M. G., Simmons, A. J., Suttie, M., Stein, O., Thépaut, J.-N., Thouret, V., Vrekoussis, M., Zerefos, C., and the MACC team: The MACC reanalysis: an 8 yr data set of atmospheric composition, Atmos.Chem. Phys., 13, 4073–4109, doi:10.5194/acp-13-4073-2013, 2013.

Jilbert, T., Reichart, G.-J., Aeschlimann, B., Günther, D., Boer, W. and de Lange, G.: Climate-controlled multidecadal variability in North African dust transport to the Mediterranean, Geology, 38, 19–22, doi: 10.1130/G25287.1, 2010.

Jones, C., Mahowald, N., and Luo, C.: The role of easterly waves on African desert dust transport, J. Climate, 16, 3617–3628, 2003.

Kahn, R. A., Gaitley, B. J., Garay, M. J., Diner, D. J., Eck, T. F., Smirnov, A., and Holben B. N.: Multiangle Imaging SpectroRadiometer global aerosol product assessment by comparison with the Aerosol Robotic Network, J. Geophys. Res., 115, D23209, doi:10.1029/2010JD014601, 2010.

Kalnay, E., Kanamitsu, M., Kistler, R., Collins, W., Deaven, D., Gandin, L., Iredell, M., Saha, S., White, G., Woollen, J., Zhu, Y., Leetmaa, A., Reynolds, R., Chelliah, M., Ebisuzaki, W., Higgins, W., Janowiak, J., Mo, K. C., Ropelewski, C., Wang, J., Jenne, R., and Joseph, D.: The NCEP/NCAR 40-Year Reanalysis Project, B. Am. Meteorol. Soc., 77, 437–471, 1996.

Karoly, D. J., and Hoskins, B. J.: 3 dimensional propagation of planetary-waves, Journal of the Meteorological Society of Japan, 60, 109-123, 1982.

Karoly, D. J.: Rossby-wave propagation in a barotropic atmosphere, Dynamics of Atmospheres and Oceans, 7, 111-125, 10.1016/0377-0265(83)90013-1, 1983.

Kaufman, Y. J., Tanré, D., Remer, L. A., Vermote, E. F., Chu, A., Holben, B. N.: Operational remote sensing of tropospheric aerosol over land from EOS moderate resolution imaging spectroradiometer, J. Geophys. Res., 102, 17–51, 1997.

Knippertz, P.: Dust emissions in the West African heat trough—The role of the diurnal cycle and of extratropical disturbances, Meteorol. Z.,17(5), 553–563, 2008.

Knippertz, P., and Todd, M.C.: The central west Saharan dust hot spot and its relation to African easterly waves and extratropical disturbances, J. Geophys. Res., 115, D12117, doi:10.1029/2009JD012819, 2010.

Kubilay, N., Cokacar, T., and Oguz, T.: Optical properties of mineral dust outbreaks over the northeastern Mediterranean, J. Geophys. Res., 108(D21), 4666, doi:10.1029/2003JD003798, 2003.

Lavaysse, C., Flamant, C., Janicot, S., Parker, D.J., Lafore, J.-P., Sultan, B., and Pelon, J.: Seasonal evolution of the West African heat low: A climatological perspective. Clim. Dyn. 33, 313–330, 2009.

Lavaysse, C., Flamant, C., and Janicot, S.: Regional-scale convection patterns during strong and weak phases of the Saharan heat low, Atmos. Sci. Lett., 11, 255–264, doi:10.1002/asl.284, 2010a.

Lavaysse, C., Flamant, C., Janicot, S., and Knippertz, P: Links between African easterly waves, mid-latitude circulation and the intra seasonal pulsations of the West African Heat Low, Quart. J. Roy. Meteor. Soc., 136, 141 – 158, DOI: 10.1002/qj.555, 2010b.

Lavaysse, C., Chaboureau, J.-P., and Flamant, C.: Dust impact on the West African heat low in summertime, Quart. J. Roy. Meteor. Soc., 137, 1227–1240, doi:10.1002/qj.844, 2011.

Lavaysse, C., Eymard, L., Flamant, C., Karbou, F., Mimouni, M., and Saci, A.: Monitoring the West African heat low at seasonal and intra-seasonal timescales using AMSU-A sounder. Atmospheric Science Letters 14, 263-271, 2013.

Lavaysse, C., Flamant, C., Evan, A., Janicot, S., and Gaetani, M.: Recent climatological trend of the Saharan heat low and its impact on the West African climate, Climate Dyn., p. in press, 715 doi:10.1007/s00382-015-2847-z, 2015.

Marsham, J., Parker, D. Grams, C., Taylor, C., and Haywood, J.: Uplift of Saharan dust south of the intertropical discontinuity, J. Geophys. Res., 113, D21102, doi:10.1029/2008JD009844, 2008.

Marsham, J. H., Hobby, M., Allen, C. J. T., Banks, J. R., Bart, M., Brooks, B. J., Cavazos-Guerra, C., Engelstaedter, S., Gascoyne, M., Lima, A. R., Martins, J. V., McQuaid, J. B., O'Leary, A., Ouchene, B., Ouladichir, A., Parker, D. J., Saci, A., Salah-Ferroudj, M., Todd, M. C., and Washington, R.: Meteorology and dust in the central Sahara: Observations from Fennec supersite-1 during the June 2011 intensive observation period, J. Geophys. Res., 118, 4069–4089, doi:10.1002/jgrd.50211, 2013.

Marconi, M., Sferlazzo, D. M., Becagli, S., Bommarito, C., Calzolai, G., Chiari, M., di Sarra, A., Ghedini, C., Gómez-Amo, J. L., Lucarelli, F., Meloni, D., Monteleone, F., Nava, S., Pace, G., Piacentino, S., Rugi, F., Severi, M., Traversi, R., and Udisti, R.: Saharan dust aerosol over the central Mediterranean Sea: PM10 chemical composition and concentration versus optical columnar measurements, Atmos. Chem. Phys., 14, 2039-2054, doi:10.5194/acp-14-2039-2014, 2014.

Marticorena, B., Chatenet, B., Rajot, J. L., Traoré, S., Coulibaly, M., Diallo, A., Koné, I., Maman, A., NDiaye, T., and Zakou, A.: Temporal variability of mineral dust concentrations over West Africa: analyses of a pluriannual monitoring from the AMMA Sahelian Dust Transect, Atmos. Chem. Phys., 10, 8899–8915, doi:10.5194/acp-10-8899-2010, 2010.

Mona, L., Amodeo, A., Pandolfi, M., Pappalardo, G.: Saharan dust intrusions in the Mediterranean area: Three years of Raman lidar measurements, J. Geophys. Res. 111, D16203, doi: 10.1029/2005JD006569, 2006.

Morcrette, J.-J., Boucher, O., Jones, L., Salmond, D., Bechtold, P., Beljaars, A., Benedetti, A., Bonet, A., Kaiser, J. W., Razinger, M., Schulz, M., Serrar, S., Simmons, A. J., Sofiev, M., Suttie, M., Tompkins, A. M., and Untch, A.: Aerosol analysis and forecast in the ECMWF integrated forecast system. Part I: Forward modelling, J. Geophys. Res., 114, D06206, doi:10.1029/2008JD011235, 2009.

Morcrette, J.-J., Benedetti, A., Jones, L., Kaiser, J. W., Razinger, M., and Suttie, M.: Prognostic Aerosols in the ECMWF IFS: MACC vs. GEMS Aerosols, ECMWF Tech Memo 659, available at: http://old.ecmwf.int/publications/library/ecpublications/_pdf/ tm/601-700/tm659.pdf (last access: 4 November 2014), 2011.

Moulin, C., Lambert, C. E., Dayan, U., Masson, V., Ramonet, M., Bousquet, P., Legrand, M., Balkanski, Y. J., Guelle, W., Marticorena, B., Bergametti, G., and Dulac, F.: Satellite climatology of African dust transport in the Mediterranean atmosphere, J. Geophys. Res., 103, 13137–13144, 1998.

Pérez, C., Nickovic, S., Baldasano, J. M., Sicard, M., Rocadenbosch, F., and Cachorro, V. E.: A long Saharan dust event over the western Mediterranean: Lidar, Sun photometer observations, and regional dust modeling, J. Geophys. Res., 111, doi:10.1029/2005JD006579, 2006.

Pedlosky, J.: Geophysical Fluid Dynamics, Second edition, Springer-Verlag, New York, 1987.

Perry, K. D., Cahill, T. A., Eldred, R. A., Dutcher, D. D., and Gill, T. E.: Long-range transport of North African dust to the eastern United States, J. Geophys. Res., 102, D10, 11225–11238, doi:10.1029/97JD00260, 1997.

Petoukhov, V., Rahmstorf, S., Petri, S., and Schellnhuber, H. J.: Quasiresonant amplification of planetary waves and recent Northern Hemisphere weather extremes, Proceedings of the National Academy of Sciences of the United States of America, 110, 5336-5341, doi:10.1073/pnas.1222000110, 2013.

Press, W. H., Teukolsky, S. A., Vetterling, W. T., and Flannery, B. P.: Numerical Recipes in FORTRAN. The Art of Scientific Computing, Second edition reprinted with corrections, Cambridge University Press, Cambridge, 1994

Prospero, J. M. and Carlson, T. N.: Vertical and areal distribution of Saharan dust over the western Equatorial North Atlantic Ocean, J. Geophys. Res., 77, 5255–5265, 1972.

Prospero, J.M.: Long-range transport of mineral dust in the global atmosphere: Impact of African dust on the environment of the southeastern United States, PNAS, 96, 7, 3396–3403, doi: 10.1073/pnas.96.7.3396, 1999.

Prospero, J. M. and Lamb, P. J.: African droughts and dust transport to the Caribbean: climate change implications, Science, 302, 1024–1027, doi:10.1126/science.1089915, 2003.

Prospero, J. M., Collard, F.-X., Molinié, J., and Jeannot, A.: Characterizing the annual cycle of African dust transport to the Caribbean Basin and South America and its impact on the environment and air quality, Global Biogeochem. Cycles, 29, doi:10.1002/2013GB004802, 2014.

Querol, X., Pey, J., Pandolfi, M., Alastuey, A., Cusack, M., Pérez, N., Moreno, N., Viana, M., Mihalopoulos, N., Kallos, G., and Kleanthous, S.: African dust contributions to mean ambient PM10 mass-levels across the Mediterranean basin, Atmos. Environ., 43, 4266–4277, 2009.

Ravelo-Pérez, L.M., Rodríguez, S., Galindo, L., García, M.I., Alastuey, A., López-Solano, J.: Soluble iron dust export in the high altitude Saharan Air Layer, Atmospheric Environment, 133, 49–59, 2016.

Reddy, M. S., Boucher, O., Bellouin, N., Schulz, M., Balkanski, Y., Dufresne, J.-L., and Pham, M.: Estimates of global multi-component aerosol optical depth and direct radiative perturbation in the Laboratoire de Météorologie Dynamique general circulation model, J. Geophys. Res., 110, D10S16, doi:10.1029/2004JD004757, 2005.

Ridley, D. A., Heald, C. L., and Prospero, J. M.: What controls the recent changes in African mineral dust aerosol across the Atlantic?, Atmos. Chem. Phys., 14, 5735–5747, doi:10.5194/acp-14-5735-2014, 2014.

Roehrig, R., Chauvin, F., and Lafore, J.-P.: 10-25-Day intraseasonal variability of convection over the Sahel: A role of the Saharan heat low and midlatitudes, J. Clim., 24(22), 5863–5878, doi:10.1175/2011JCLI3960.1., 2011.

Rodríguez, S., Querol, X., Alastuey, A., Kallos, G., and Kakaliagou, O.: Saharan dust contributions to PM10 and TSP levels in Southern and Eastern Spain, Atmos. Environ., 35, 2433–2447, 2001.

Rodríguez, S., Cuevas, E., Prospero, J. M., Alastuey, A., Querol, X., López-Solano, J., García, M. I., and Alonso-Pérez, S.: Modulation of Saharan dust export by the North African dipole, Atmos. Chem. Phys., 15, 7471-7486, doi:10.5194/acp-15-7471-2015, 2015.

Salomonson, V. V., Barnes, W. L., Maymon, P. W., Montgomery,H. E., and Ostrow, H.: MODIS: advanced facility instrument for studies of the Earth as a system, IEEE T. Geosci. Remote, 27, 145–153, 1989.

Salvador, P., Alonso-Pérez, S., Pey, J., Artíñano, B., de Bustos, J. J., Alastuey, A., and Querol, X.: African dust outbreaks over the western Mediterranean Basin: 11-year characterization of atmospheric circulation patterns and dust source areas, Atmos. Chem. Phys., 14, 6759-6775, doi:10.5194/acp-14-6759-2014, 2014.

Sayer, A. M., Hsu, N. C., Bettenhausen, C., and Jeong, M.-J.: Validation and uncertainty estimates for MODIS Collection 6 "Deep Blue" aerosol data, J. Geophys. Res. Atmos., 118, 7864–7872, doi:10.1002/jgrd.50600, 2013.

Schepanski, K., Tegen, I., Todd, M. C., Heinold, B., Bönisch, G., Laurent, B., and Macke, A.: Meteorological processes forcing Saharan dust emission inferred from MSG-SEVIRI observations of subdaily dust source activation and numerical models, J. Geophys. Res., 114, D10201, doi:10.1029/2008JD010325, 2009.

Stein, A.F., Draxler, R.R, Rolph, G.D., Stunder, B.J.B., Cohen, M.D., and Ngan, F.: NOAA's HYSPLIT atmospheric transport and dispersion modeling system, Bull. Amer. Meteor. Soc., 96, 2059-2077, http://dx.doi.org/10.1175/BAMS-D-14-00110.1, 2015.

Tanré, D., Kaufman, Y. J., Herman, M., and Mattoo, S.: Remote sensing of aerosol properties over oceans using the MODIS/EOS spectral radiances, J. Geophys. Res., 102, 16971–16988, doi:10.1029/96JD03437, 1997.

Varga, G., Ùjvári, G, Kovács, J.: Spatiotemporal patterns of Saharan dust outbreaks in the Mediterranean Basin, Aeolian Res., 15, 151–160, doi:10.1016/j.aeolia.2014.06.005, 2014.

Wang, W., A. T. Evan, C. Flamant, C. Lavaysse: On the decadal scale correlation between African dust and Sahel rainfall: The role of Saharan heat low–forced winds, Sci. Adv. 1, e1500646, 2015.

Atmos. Chem. Phys. Discuss., doi:10.5194/acp-2016-287, 2016
Manuscript under review for journal Atmos. Chem. Phys.
Published: 22 April 2016

Atmospheric Chemistry and Physics
Discussions
Open Access

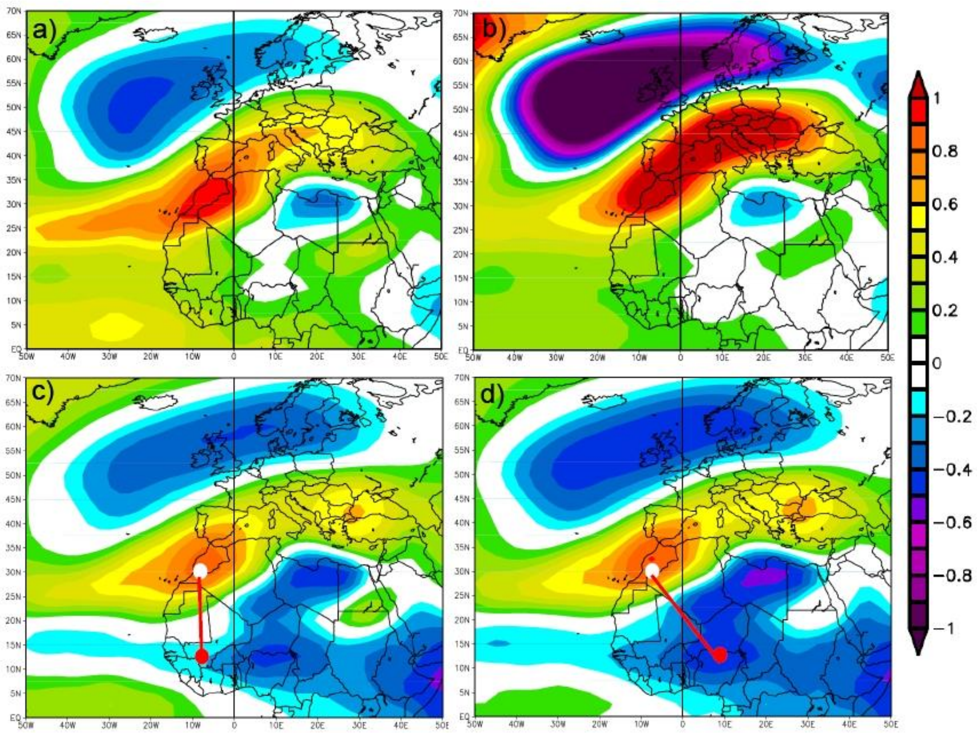

Figure 1. NCEP monthly correlation and regression plots for August months of the period 1980-2013: a) correlation between the geopotential height at 700 hPa over Morocco and the geopotential height field at 700 hPa; b) regression between the geopotential height at 700 hPa over Morocco and the geopotential height field at 700 hPa; c) correlation between the former NAFDI and the geopotential height field at 700 hPa; and d) correlation between the improved NAFDI and the geopotential height field at 700 hPa.

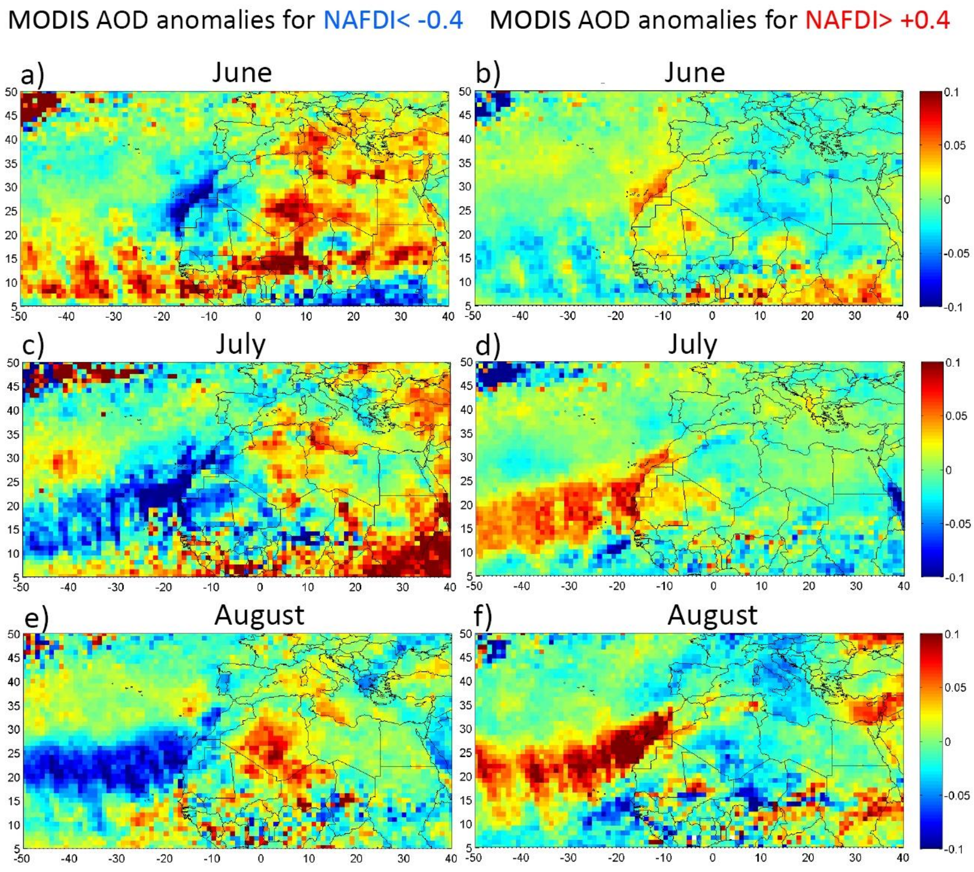

Figure 2. Averaged AOD anomalies from combined MODIS Dark-Target and Deep-Blue AOD at 550 nm for summer months (June, July and August) with positive and negative NAFDI phases, in the period 2003-2012. These plots were obtained by averaging the AOD anomalies for each month and each phase of the NAFDI.

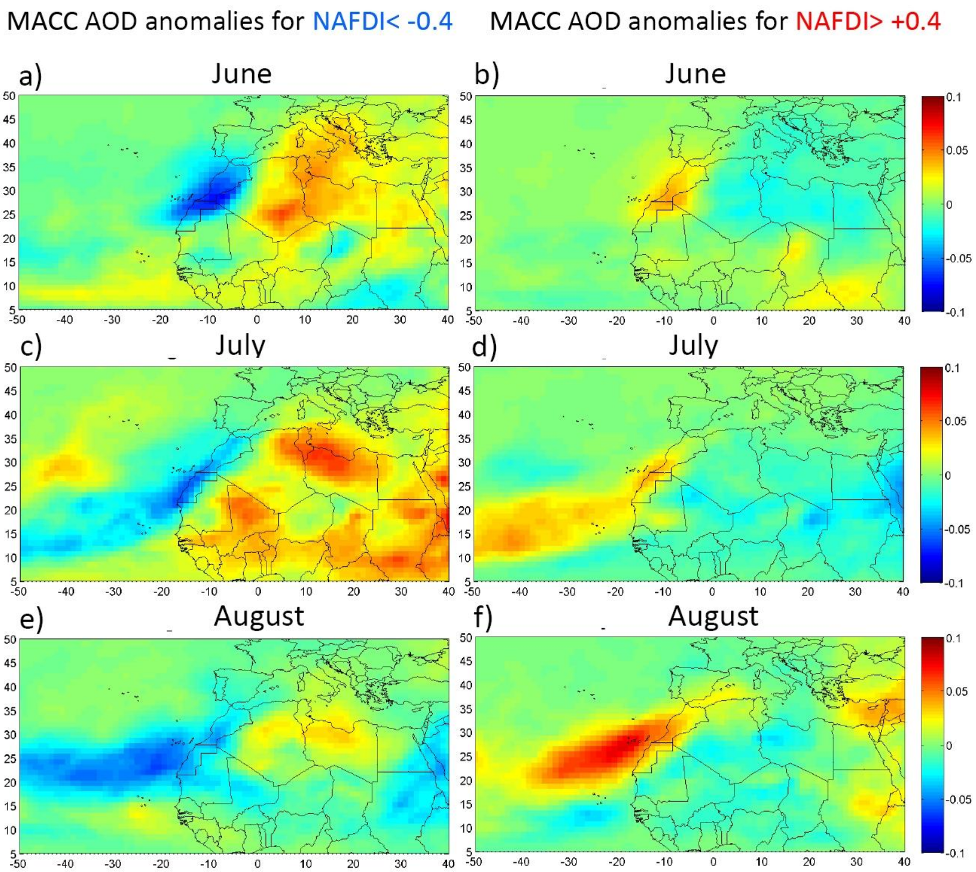

Figure 3. Averaged AOD anomalies from MACC reanalysis AOD at 550 nm for summer months (June, July and August) with positive and negative NAFDI phases, in the period 2003-2012. These plots were obtained by averaging the AOD anomalies for each month and each phase of the NAFDI.

Atmos. Chem. Phys. Discuss., doi:10.5194/acp-2016-287, 2016
Manuscript under review for journal Atmos. Chem. Phys.
Published: 22 April 2016

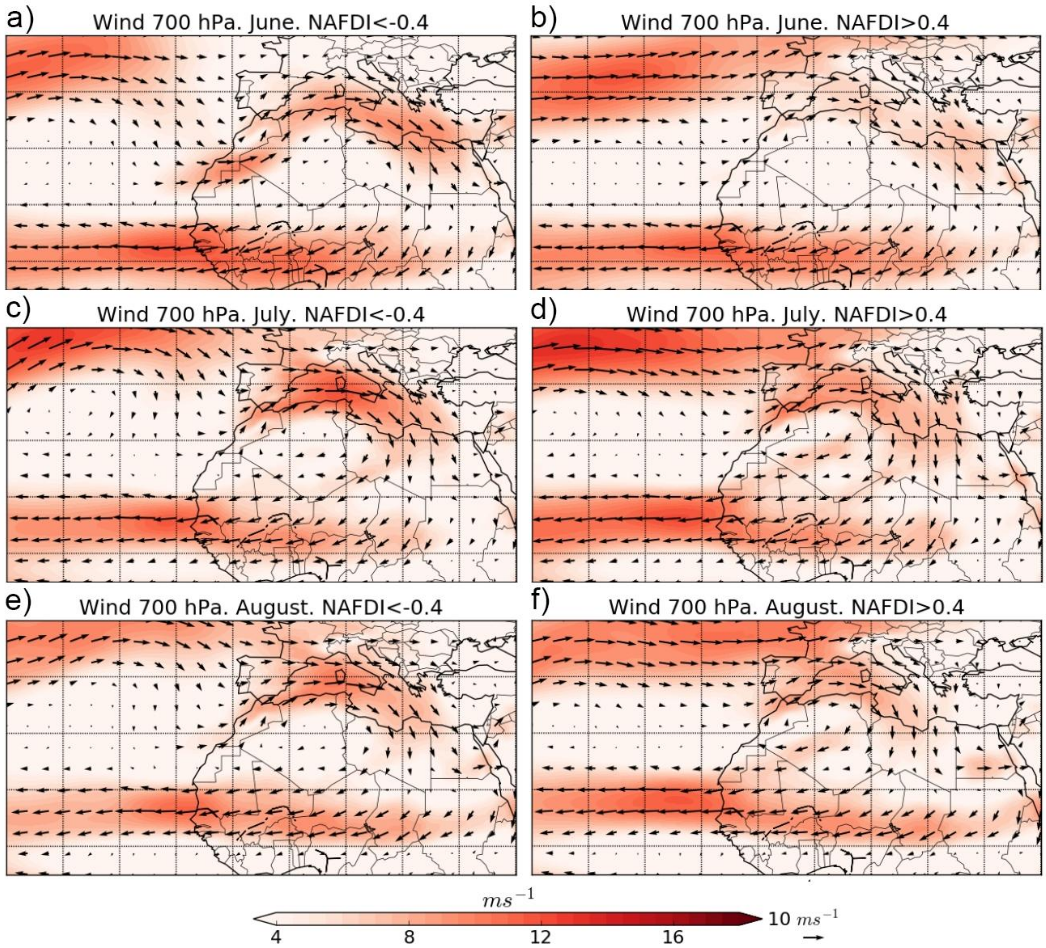

Figure 4. Monthly averages of ECMWF wind vector and speed at 700 hPa for summer months (June, July and August) with positive and negative NAFDI phases, in the period 2003-2012.

Atmos. Chem. Phys. Discuss., doi:10.5194/acp-2016-287, 2016
Manuscript under review for journal Atmos. Chem. Phys.
Published: 22 April 2016

Atmospheric Chemistry and Physics
Open Access
Discussions

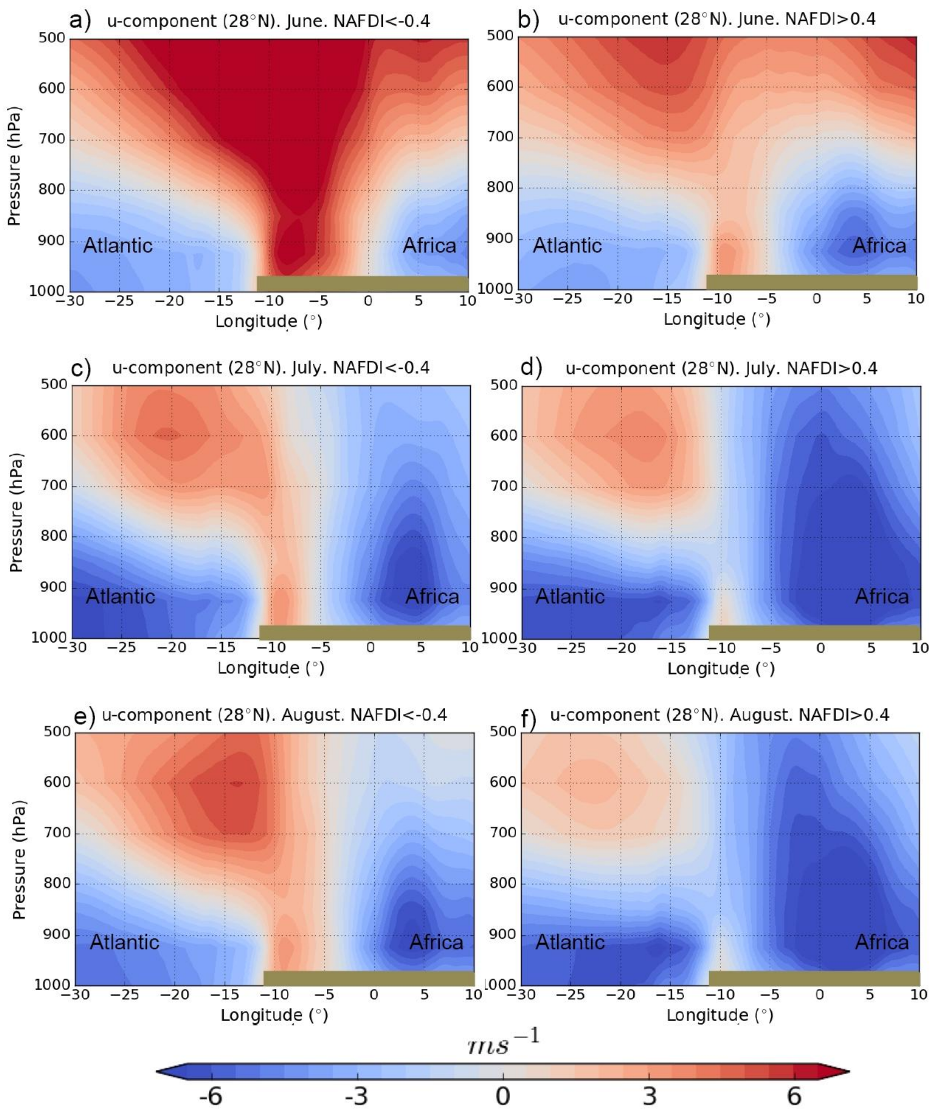

Figure 5. Monthly means of ECMWF zonal wind height-longitude cross-sections along the 28°N parallel (Subtropical North Atlantic and Western Sahara) for June, July, and August (2003-2012), and for negative (a, c, and e) and positive (b, d, and f) NAFDI, respectively.

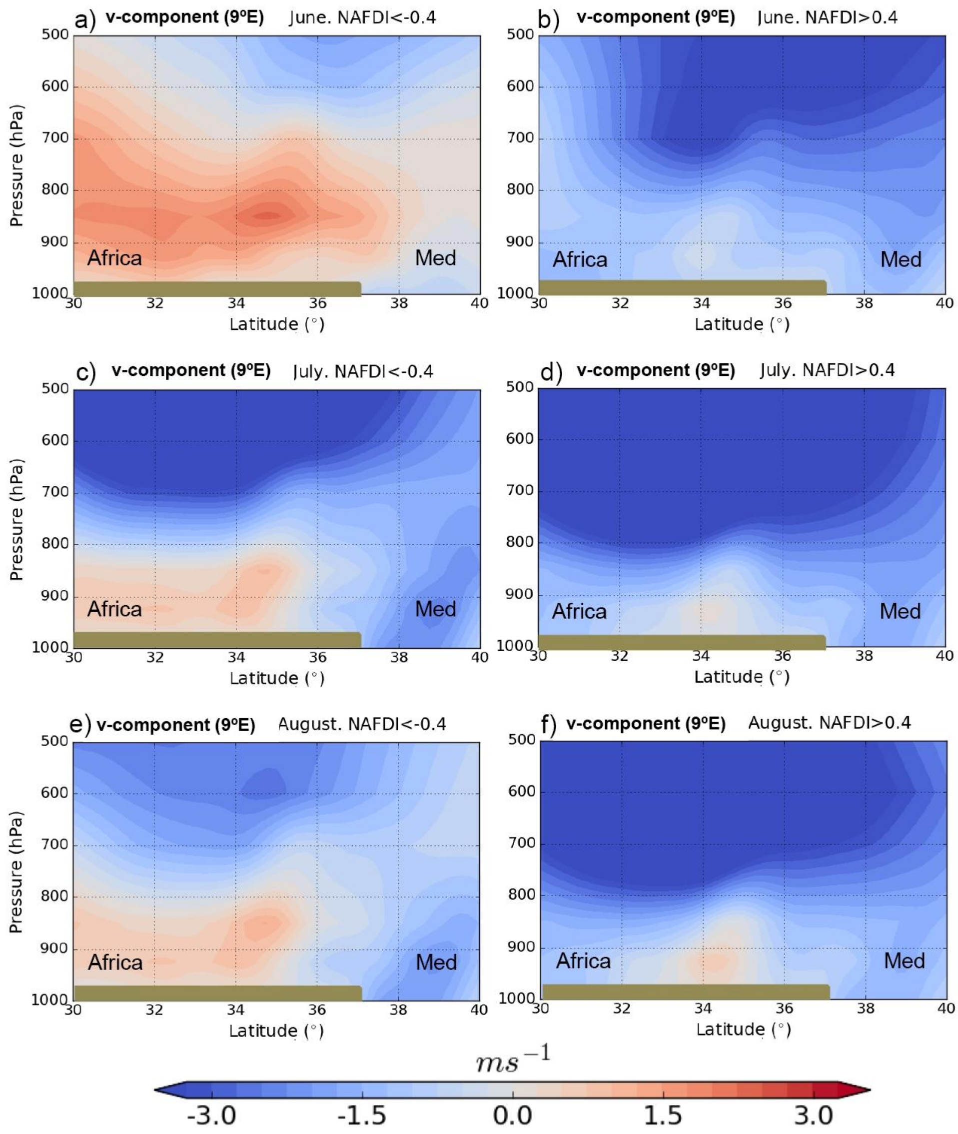

Figure 6. Monthly means of ECMWF meridional wind height-latitude cross-sections along the 9°E meridian (Central-West Mediterranean and Northern Africa) for June, July, and August (2003-2012), and for negative (a, c, and e) and positive (b, d, and f) NAFDI, respectively.

Atmos. Chem. Phys. Discuss., doi:10.5194/acp-2016-287, 2016
Manuscript under review for journal Atmos. Chem. Phys.
Published: 22 April 2016

Atmospheric Chemistry and Physics
Discussions

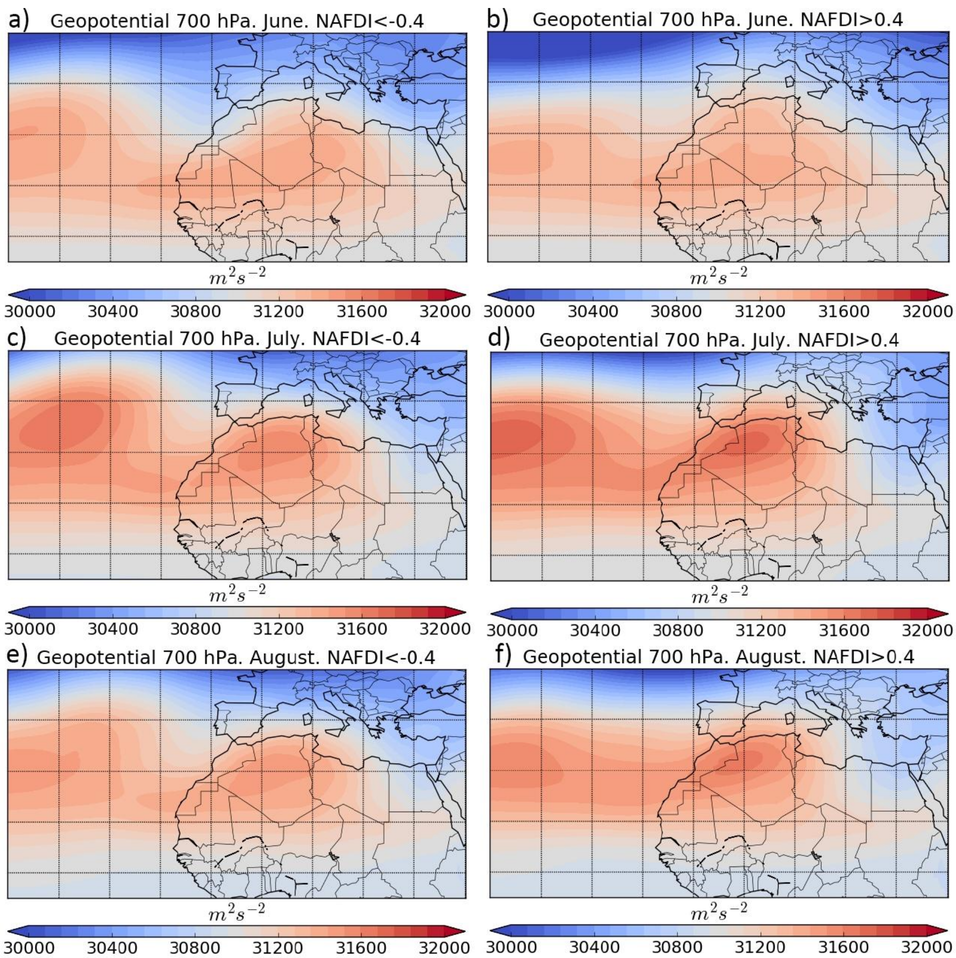

Figure 7. Monthly averages of ECMWF geopotential height at 700 hPa for summer months (June, July and August) with positive and negative NAFDI phases, in the period 2003-2012.

Atmos. Chem. Phys. Discuss., doi:10.5194/acp-2016-287, 2016
Manuscript under review for journal Atmos. Chem. Phys.
Published: 22 April 2016

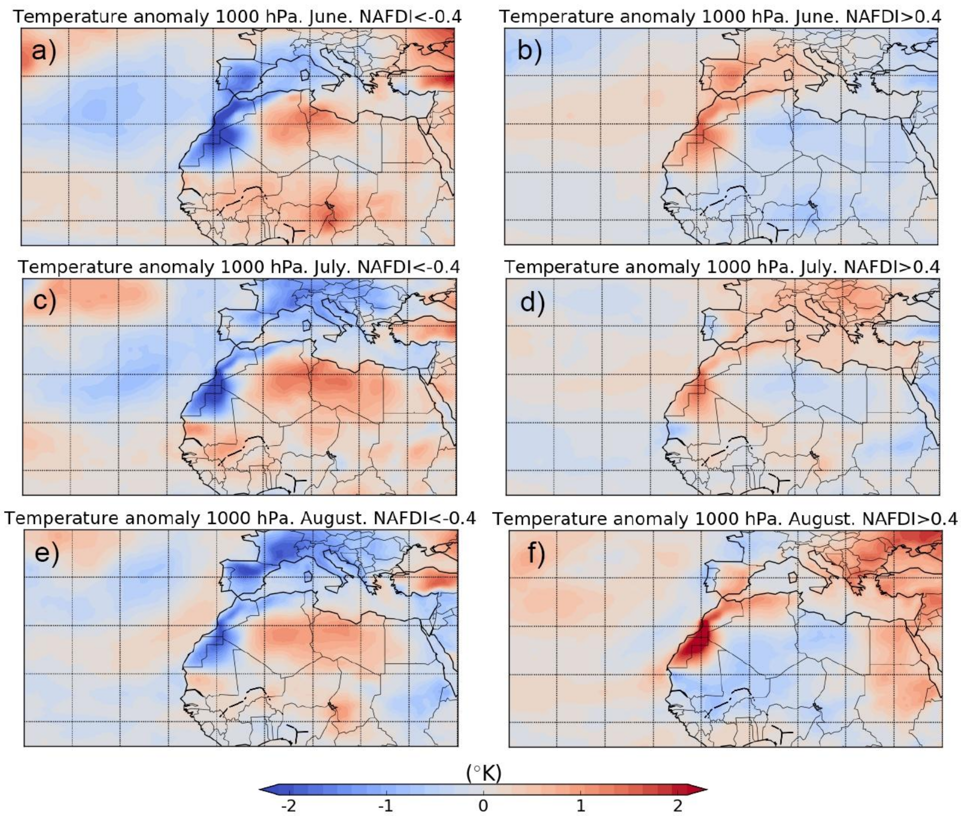

Figure 8. Monthly averages of ECMWF temperature anomalies at 1000 hPa for summer months (June, July and August) with positive and negative NAFDI phases, in the period 2003-2012.

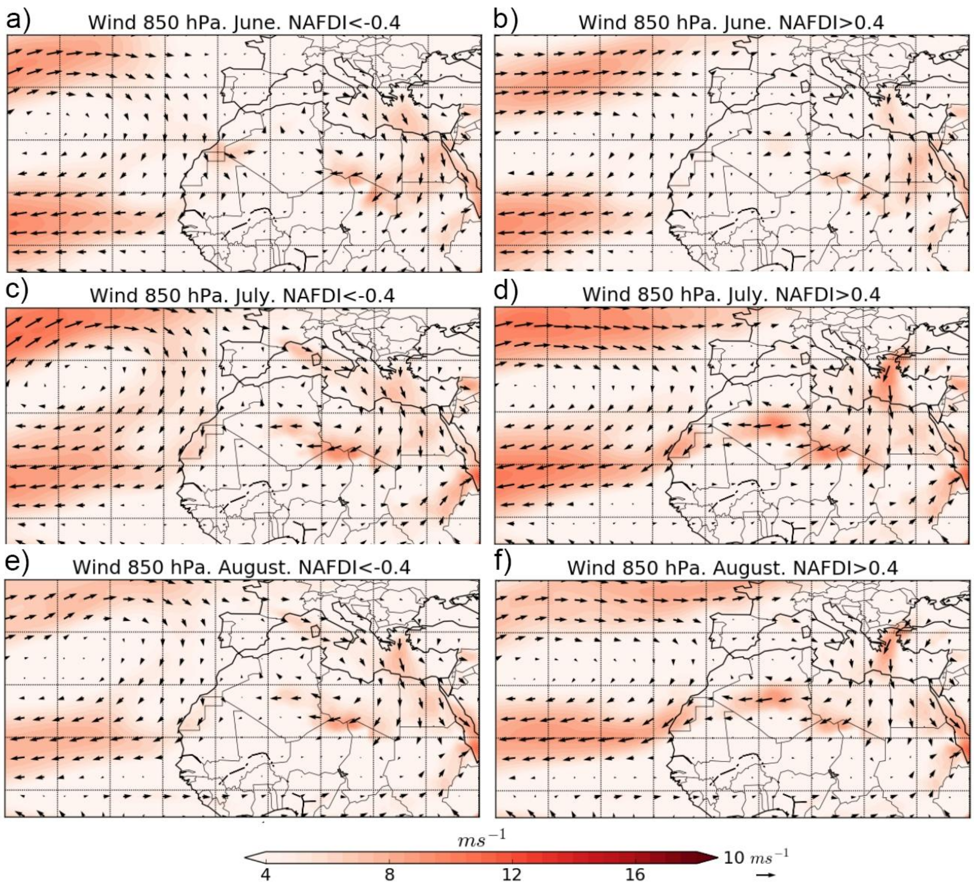

Figure 9. Monthly averages of ECMWF wind vector and speed at 850 hPa for summer months (June, July and August) with positive and negative NAFDI phases, in the period 2003-2012.

Atmos. Chem. Phys. Discuss., doi:10.5194/acp-2016-287, 2016
Manuscript under review for journal Atmos. Chem. Phys.
Published: 22 April 2016

Atmospheric Chemistry and Physics
Discussions
Open Access

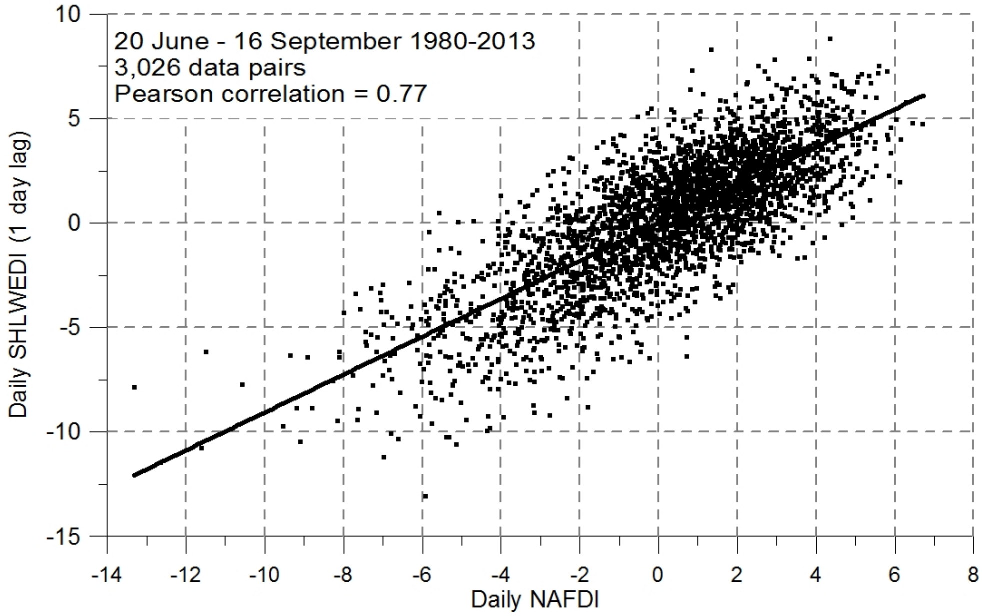

Figure 10. Daily NAFDI vs Daily SHLWEDI 1-day lag for 20 June – 16 September 1980-2013.

Atmos. Chem. Phys. Discuss., doi:10.5194/acp-2016-287, 2016
Manuscript under review for journal Atmos. Chem. Phys.
Published: 22 April 2016

Atmospheric Chemistry and Physics
Open Access
Discussions

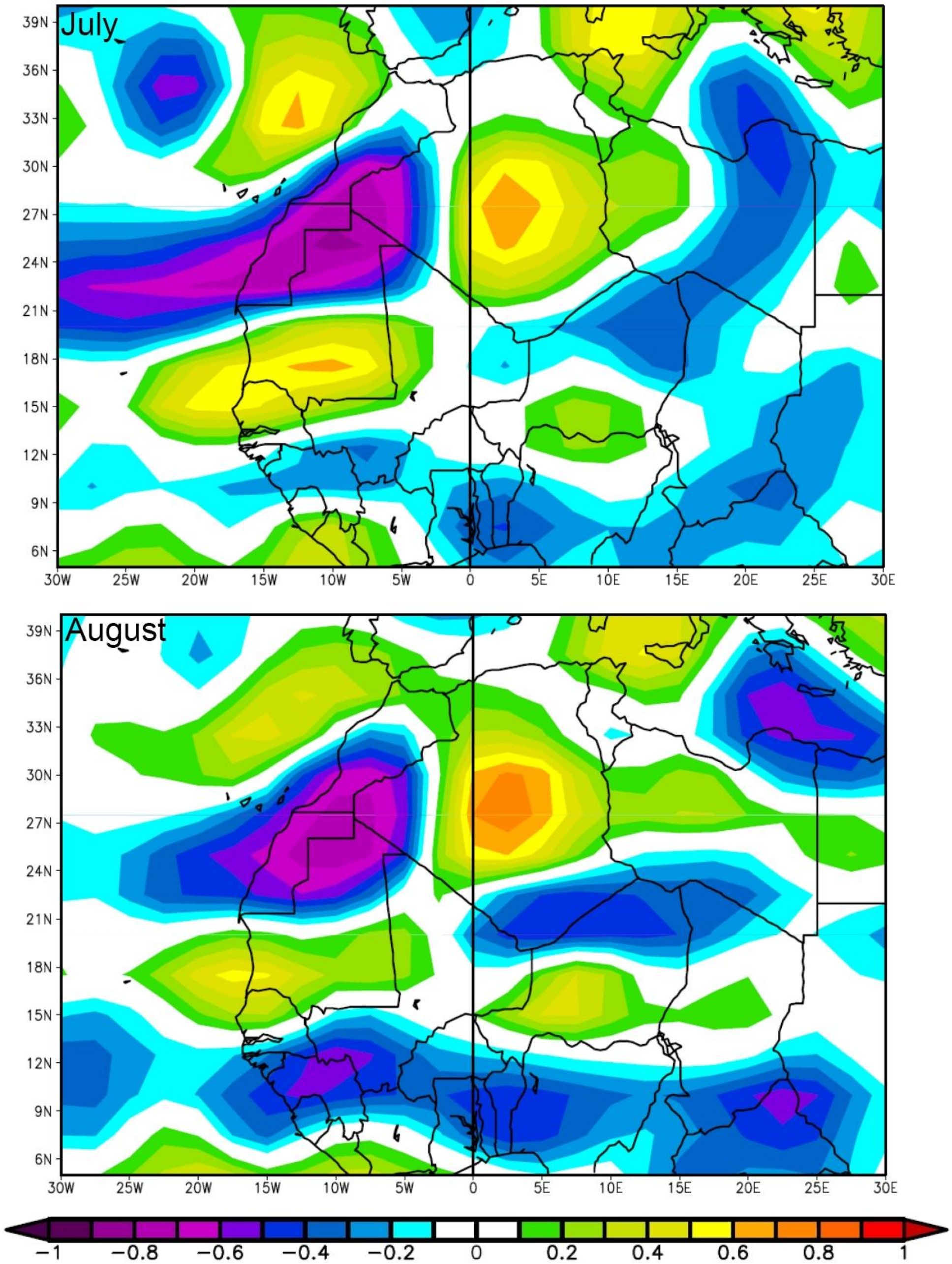

Figure 11. Correlation plots between NAFDI and Omega at 850 hPa for July (upper panel) and August (lower panel) for the period 1980-2013.

Atmos. Chem. Phys. Discuss., doi:10.5194/acp-2016-287, 2016
Manuscript under review for journal Atmos. Chem. Phys.
Published: 22 April 2016

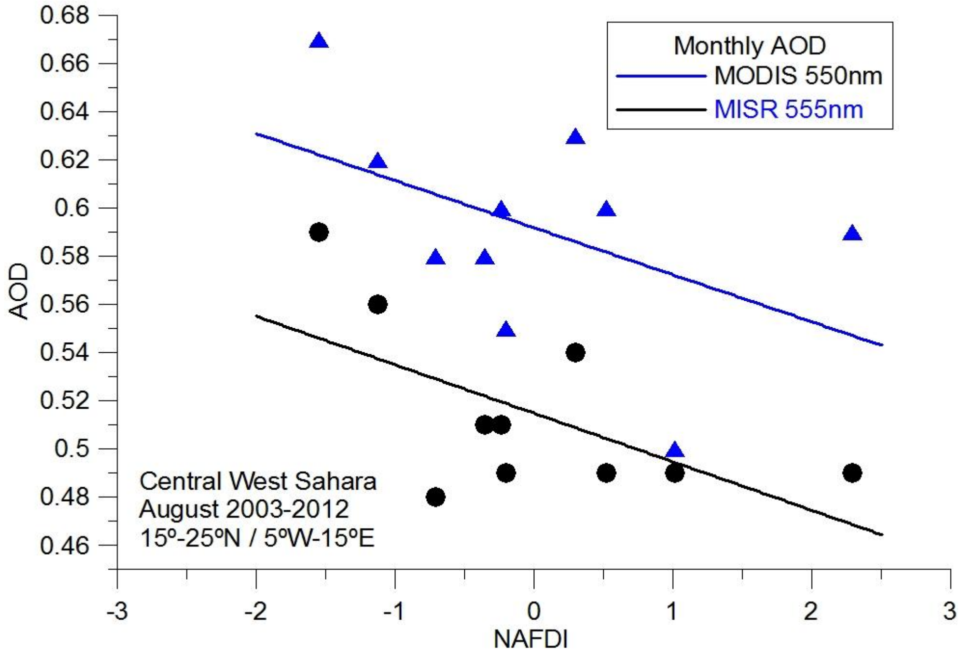

Figure 12. AOD monthly means for August months in the period 2003-2012, from MODIS and MISR data over the 15º-25ºN / 5ºW-15ºE region in central west Sahara. The straight lines represent least-square fits to the monthly means.

Atmos. Chem. Phys. Discuss., doi:10.5194/acp-2016-287, 2016
Manuscript under review for journal Atmos. Chem. Phys.
Published: 22 April 2016

Atmospheric Chemistry and Physics Discussions

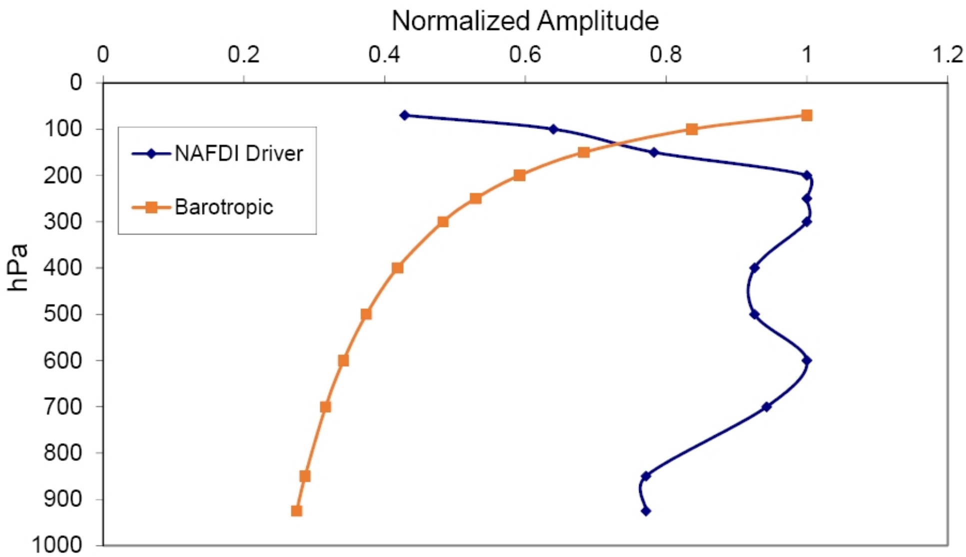

Figure 13. Vertical profile of the normalized amplitude for a pure free barotropic Rossby wave (in an isothermal atmosphere with a uniform zonal flow) and for the real Rossby wave that drives the NAFDI variations.

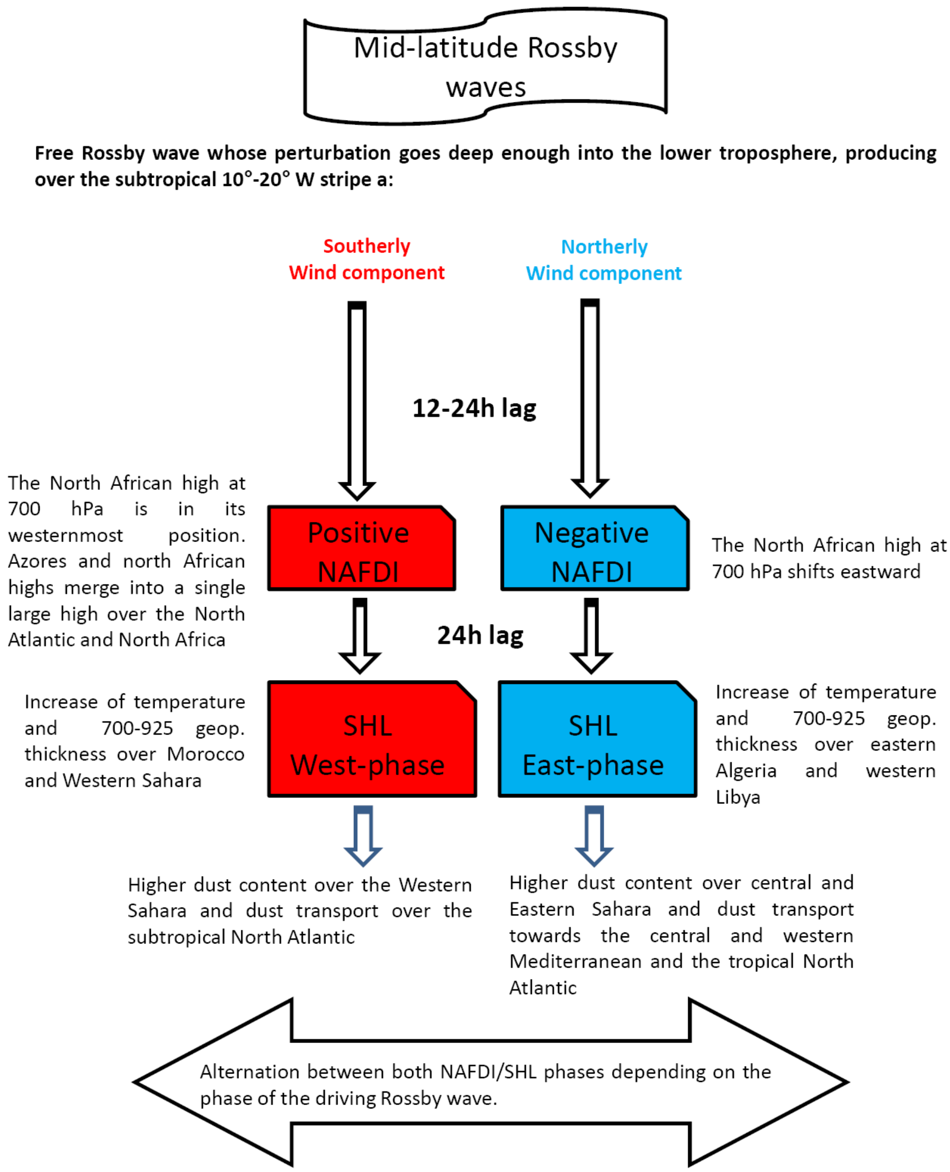

Figure 14. Scheme of the comprehensive top-down atmospheric conceptual model: from hemispheric to mesoscale atmospheric mechanisms driving dust mobilization and transport over Northern Africa.